

Strong Primary Contribution to Brown Carbon Light Absorption in Tibet and Urban Areas:

Insights based on in situ measurements

Wenhui Zhao^{1,2}, Weiwei Hu^{1,3,4*}, Zhaoce Liu^{1,2}, Tianle Pan^{1,2}, Tingting Feng^{1,2}, Jun Wang^{1,2}, Yiyu Cai^{1,2}, Lin Liang^{5,6}, Shan Huang^{5,6*}, Bin Yuan^{5,6}, Nan Ma^{5,6}, Min Shao^{5,6}, Guohua Zhang^{1,3,4}, Xinhui Bi^{1,3,4}, Ximeng Wang^{1,3,4}, Pengfei Yu^{5,6}

1. State Key Laboratory of Advanced Environmental Technology, Guangzhou Institute of Geochemistry, Chinese Academy of Sciences, Guangzhou, 510640, China;

2. University of Chinese Academy of Sciences, Beijing 100049, China;

3. Guangdong–Hong Kong–Macao Greater Bay Area Environmental Pollution Research and Control Joint Laboratory, Guangzhou Institute of Geochemistry, Chinese Academy of Sciences, Guangzhou 510640, China;

4. Guangdong Key Laboratory of Environmental Resource Utilization and Protection, Guangzhou Institute of Geochemistry, Chinese Academy of Sciences, Guangzhou 510640, China;

5. College of Environment and Climate, Jinan University, Guangzhou 511443, China;

6. Guangdong–Hongkong–Macau Joint Laboratory of Collaborative Innovation for Environmental Quality, Guangzhou 511443, China

*Correspondence to: WeiweiHu@gig.ac.cn; shanhuang_eci@jnu.edu.cn

1 **Abstract**

2 To investigate optical properties, sources, and radiative effects of brown carbon (BrC), we
3 conducted synchronous field campaigns in the Qinghai–Tibet Plateau (Yangbajing) and urban
4 Guangzhou in July 2022, using multi-wavelength Aethalometer (AE33) and aerosol mass spectrometer
5 (AMS) measurements. Total aerosol and BrC light absorption coefficients at 370 nm ($\text{Abs}_{\text{total}}$: 1.6 ± 1.6
6 M m^{-1} ; BrC: $0.2 \pm 0.3 \text{ M m}^{-1}$) in Tibet were an order of magnitude lower than Guangzhou, attributed to
7 extremely low aerosol/organic aerosol (OA) mass concentrations. However, BrC fractions in $\text{Abs}_{\text{total}}$ (15 %
8 vs. 21 % at 370 nm) correlated with primary OA (POA) ratios, highlighting anthropogenic emission
9 impacts even in this clean background. Diurnal variations (morning/evening peaks) of source–specific
10 BrC absorption were regulated by local emissions (e.g., biomass burning, traffic emission) and regional
11 secondary formation. Source apportionment revealed primary sources (biomass burning OA (BBOA),
12 hydrocarbon-like OA (HOA)) dominated BrC absorption (> 75 %). The mass absorption cross–section
13 (MAC) of HOA ($2.08 \text{ m}^2 \text{ g}^{-1}$ in Tibet; $2.57 \text{ m}^2 \text{ g}^{-1}$ in Guangzhou) was comparable to that of BBOA (1.11–
14 2.54 in Tibet; $1.91 \text{ m}^2 \text{ g}^{-1}$ in Guangzhou), indicating the high light absorption capacity of BrC from fossil
15 fuel. Integrated "simple forcing efficiency" (370–660 nm) showed primary emissions contributed > 98 %
16 of total radiative forcing at both sites. This study advances understanding of BrC dynamics and sources
17 in diverse environments, underscores primary sources' critical role in BrC absorption, and emphasizes
18 the need for source–specific OA optical parameterization.

19 **Keywords:**

20 Brown carbon; Source apportionment; Multiple linear regression; Optical properties; Radiative forcing

21 **1. Introduction**

22 Light absorbing components of atmospheric aerosols comprise black carbon (BC) and light
23 absorbing organic aerosols, known as brown carbon (BrC). The BrC exhibits significant absorption in
24 the near-ultraviolet (300–400 nm) and visible ranges (Andreae and Gelencsér, 2006; Kirchstetter and
25 Thatcher, 2012; Laskin et al., 2015), but it remains largely overlooked in most climate models (Chung et
26 al., 2012). Feng et al. (2013) found that accounting for the strong absorption of BrC in model could shift
27 the global mean direct radiative forcing of OA at the top of the atmosphere from a cooling of -0.08 W m^{-2}
28 to a warming of $+0.025 \text{ W m}^{-2}$, emphasizing the significant role of BrC in global and regional direct
29 radiative forcing of carbonaceous aerosols. Wang et al. (2025) revealed that dark BrC, emitted by
30 wildfires and agricultural burning, strongly absorbs solar radiation, thereby generating a radiative effect
31 of $+0.02$ to $+0.68 \text{ W m}^{-2}$, which contributed comparable warming as BC. Current global model simulation
32 studies have demonstrated that the impact of BrC can contribute 12–50 % of the total positive radiative
33 forcing from light-absorbing atmospheric aerosols and can be regionally different, which emphasizes the
34 spatially dynamic variation of BrC and its important role in atmospheric warming (Li et al., 2025; Brown
35 et al., 2018; Feng et al., 2013; Wang et al., 2018; Xu et al., 2024),.

36 In general, the source of atmospheric BrC can be categorized by direct emission (primary BrC) and
37 secondary generation (secondary BrC) (Laskin et al., 2015). Over the past decade, primary BrC was
38 found to be dominated by biomass burning, and the absorption capacity of BrC from fossil fuel is often
39 neglected (Saleh, 2020). However, more and more recent studies have shown that fossil fuels (vehicle
40 emissions and coal combustions) are also important contributors to the BrC, which have been previously
41 underestimated (Du et al., 2014; Kasthuriarachchi et al., 2020a; Xie et al., 2017; Huang et al., 2022; Tang
42 et al., 2020). Wang et al. (2022b) conducted a comprehensive review of the relationship between the
43 source and light absorption characteristics of BrC based on the measurement results in China, positing
44 that the emission and light absorption capacity of BrC from fossil fuel combustion might be comparable
45 to or even exceed those induced by biomass burning. This finding raises the question of how much
46 primary fossil and non-fossil sources contribute to ambient BrC. Regarding secondary BrC, its formation
47 involves complex gaseous, particulate, and liquid-phase reactions from diverse precursors (Laskin et al.,
48 2015). E.g., the nitro compounds formed through NO_3 oxidation or OH oxidation under high NO_x
49 chemistry can lead to a significant enhancement in light absorption within the ultraviolet-visible (UV–
50 Vis) range (Li et al., 2020; Jiang et al., 2019). Aqueous reactions of carbonyl groups with reduced
51 nitrogenous organic compounds, such as organic amines and ammonium, are also found to be important
52 BrC sources (Powelson et al., 2014; Tang et al., 2022).

53 The complex sources and multi-forming pathways of BrC make its global simulation a great
54 challenge, e.g., mass absorption cross-section (MAC), which serves as a crucial optical parameter in
55 simulating the BrC light absorption and further its radiative forcing, is still not clear due to the impact of
56 multiple factors. E.g., various studies have demonstrated that the BrC light absorption properties are
57 susceptible to the sources (Tang et al., 2020), photochemical aging (Yu et al., 2016; Wong et al., 2017;
58 Lee et al., 2014; Zhao et al., 2015), humidity (Kasthuriarachchi et al., 2020b), acidity of aerosols (Mo et
59 al., 2017; Phillips et al., 2017), and structure of chromophores (Laskin et al., 2014; Hems and Abbatt,
60 2018). In general, the MAC of secondary BrC was found to be generally lower than primary sources in
61 ambient BrC (Qin et al., 2018; Zhang et al., 2022b). Smog chamber experiments also show that the MAC
62 of aged coal combustion emission ($0.14 \pm 0.08 \text{ m}^2 \text{ g}^{-1}$) was much lower than that of primary emissions
63 ($0.84 \pm 0.54 \text{ m}^2 \text{ g}^{-1}$) (Ni et al., 2021). If the impact of the atmospheric aging on MAC is not considered
64 in the model, the simulated BrC light absorption may be overestimated by 45 % to 128 % (Li et al., 2025).
65 In addition, Li et al. (2025) pointed out that the uncertainty in the effective MAC of primary BrN (i.e.,
66 absorptive nitrogenous component of BrC) from anthropogenic and biomass burning has the greatest
67 impact (reaching ± 76 % uncertainty) on the simulated BrN light absorption, highlighting the key role of
68 source-specific MAC in the global simulation of BrC light absorption. Further clarification of the MAC
69 of BrC from different sources in the ambient air is imperative, which can greatly help to improve the
70 understanding of BrC light absorption and the model simulation. However, the total contribution to
71 ambient BrC from SOA and POA and their source-specific MAC values is still ambiguous due to varied
72 regions and circumstances, which warrants further study.

73 Due to the complexity and diversity of BrC, in conjunction with black carbon (BC), which share
74 similar combustion sources and complex mixture states (Bond and Bergstrom, 2006; Cappa et al., 2012;
75 Cappa et al., 2019), it remains challenging to measure the source-specific BrC light absorption in the

76 ambient air directly. The field measurement on ambient BrC begins with filter-based offline methods
77 using solvent (water or organic solvent) extraction (Bond and Bergstrom, 2006). One of the limits of the
78 offline technique is the low time resolution (usually 12–24 hours), which cannot reflect the dynamic
79 variation of BrC during a day. As measurement techniques have developed, online methods for aerosol
80 light absorption at different wavelengths have become available (Lack et al., 2014). The most widely
81 used instruments include multi-wavelength Aethalometers (AE31/AE33) (Drinovec et al., 2015) and
82 three-wavelength multi-pass Photo Acoustic Spectroscopy (PAS) (Lack et al., 2012). The online
83 measurements can provide dynamic variations in BrC light absorption at high time resolution (1 minute).
84 Together with source apportionment techniques, source contribution to BrC at high time resolution can
85 be obtained, which can greatly aid in understanding the dynamic characteristics of ambient BrC and its
86 sources.

87 Currently, most of the field studies focusing on ambient BrC and its sources are conducted in urban
88 areas (Qin et al., 2018; Sun et al., 2021; Wang et al., 2019b; Zhong et al., 2023), while the BrC
89 contribution in regional background areas is still limited. The Qinghai–Tibet Plateau (QTP) region,
90 spanning approximately 2.5 million square kilometers, is acknowledged as the world's highest plateau
91 (Yao et al., 2012). The atmosphere in QTP can substantially influence the climate in the world. E.g., the
92 light-absorbing carbonaceous aerosols have been identified as one of the main factors causing the
93 accelerated glacier retreat across the QTP (Usha et al., 2022; Kang et al., 2019; Chelluboyina et al., 2024).
94 Compared to the southern and northern regions of the QTP, anthropogenic BC is the dominant driver of
95 glaciers melt in the central QTP, whose radiative forcing can be up to 17 times greater than that in the
96 southern QTP (Li et al., 2017; Ming et al., 2013). Moreover, a portion of the glaciers in central QTP are
97 situated in the headwaters of the Yangtze River, thus, the melting directly impacts the livelihoods of
98 millions of people downstream. The melt sensitivity of these glaciers to light-absorbing impurities (such
99 as OA, BC and mineral dust) is not only higher than that of their southern counterparts but also carries
100 greater regional ecological and social significance (Li et al., 2017). Although BrC is an important light-
101 absorbing OA, limited studies on its variation and sources have been conducted in the central QTP, and
102 most have focused on the edge of the southern region (Wang et al., 2019a; Zhang et al., 2021; Tian et al.,
103 2023). We found that cross-border transport of biomass burning from South Asia was responsible for a
104 significantly higher BrC light absorption contribution in the southern QTP than in the central and
105 northeastern regions. However, OA in the central QTP not only originated from long-range transport (Xu
106 et al., 2018), but anthropogenic activities also have a significant impact on the OA sources, such as local
107 biomass burning and fossil fuels (Xiang et al., 2024). Field measurements in the central QTP can improve
108 our understanding of how human activities in remote regions impact light-absorbing aerosols and,
109 consequently, glacial melting and radiative forcing. In central QTP, only one source apportionment of the
110 light absorption of offline water-soluble BrC was reported (Zhu et al., 2024), which showed a large
111 contribution of biomass burning (29 %), fossil fuel combustion (17 %) and secondary contribution (54 %)
112 to the total BrC light absorption. Further clarification is still needed. In addition, although the online BrC
113 data have been reported in the Tibet region, the dynamic variation of BrC and its source contribution is
114 seldom shown (Zhang et al., 2021; Wang et al., 2024; Chen et al., 2024; Wang et al., 2019a; Tian et al.,
115 2023; Zhu et al., 2021; Zhu et al., 2017). The investigation of the dynamic variation of BrC, e.g., diurnal

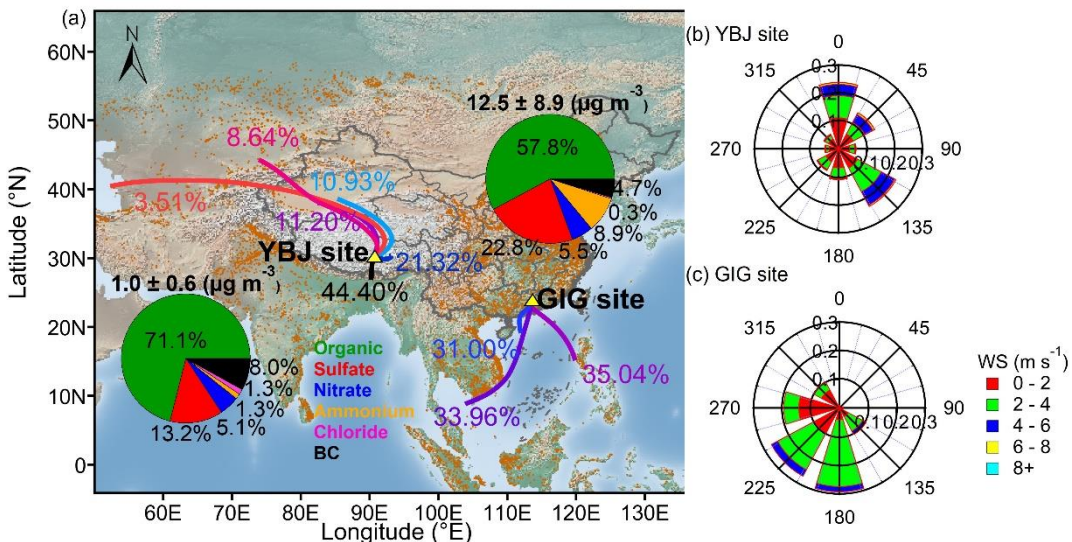
116 variation, can greatly promote the understanding of BrC fate in the ambient air, which shall be further
117 studied.

118 In this study, the real-time measurement of OA and light absorption of aerosols was carried out in
119 the background site of central QTP. For comparison, a concurrent campaign was also carried out during
120 the same period in a typical megacity of China, Guangzhou. The comparison results from distinct two
121 environments at the same time can help better understand the light absorption capacity of BrC in QTP.
122 In both campaigns, an online multi-wavelength Aethalometer (AE33) was applied to characterize the
123 dynamic variation of BrC. The positive matrix factorization (PMF) method together with aerosol mass
124 spectrometer (AMS) data was used to apportion the sources of OA. The multiple linear regression (MLR)
125 was used to explore the possible dynamic source contribution to BrC in two representative regions.
126 Finally, source-specific BrC to light absorption and the radiative forcing in remote and urban areas was
127 shown.

128 **2. Methodology**

129 **2.1. Sampling sites**

130 The field campaigns were simultaneously conducted from July 3 to August 3, 2022 in Tibet, and
131 from July 16 to August 5, 2022 in urban Guangzhou, as depicted in Fig. 1. The Yangbajing site (YBJ site;
132 30.2°N, 90.45°E; 4,300 m above sea level [a.s.l.]) serves as a background location situated in the central
133 QTP, approximately 90 km northwest of Lhasa City. With a permanent population of around 6,000, YBJ
134 was supposed to be influenced by mixed plumes of regional transportation, while local anthropogenic
135 emissions (e.g., light traffic flow and/or fuel combustion for domestic heating or cooking activities) were
136 also found (Liu et al., 2021; Xiang et al., 2024). The urban site (GIG site; 23.1 °N, 113.4°E; 53 m a.s.l.)
137 is set on the campus of the Guangzhou Institute of Geochemistry, Chinese Academy of Sciences (CAS),
138 located in the downtown area of Guangzhou (permanent population: ~20 million). The GIG site is
139 surrounded by transportation, commercial, and residential areas (Chen et al., 2021). During the whole
140 campaigns, lower temperature and Relative Humidity (RH) were observed in the YBJ site (13.4 ± 4.6 °C,
141 52.1 ± 21.9 %) than those in the GIG site (29.5 ± 2.8 °C, 82.9 ± 12.7 %), which is expected due to the
142 high altitude of Yangbajing (4,300 m) compared to Guangzhou (53 m). Southeast and north winds were
143 dominant throughout the observation period at the YBJ site with an average wind speed of 2.3 ± 1.6 m
144 s^{-1} , while the GIG site was dominated by south and southwest winds at a speed of 2.2 ± 0.9 m s^{-1} , as
145 shown in Fig. 1. The date and time used in this study are reported using Beijing Time (BJT: UTC +8h).



146
147 Figure 1. (a) Map of the locations of Yangbajing (YBJ) and Guangzhou (GIG) sites (yellow triangles).
148 Solid colored lines represent the average back trajectory clusters during the whole campaign and the
149 corresponding contributions plotted using the MeteoInfo version 2.2.6 developed by Wang (2019)
150 (download from <http://www.meteothink.org>, last access time: 23 June 2025). The orange dots on the map
151 indicate the location of the fire spot (download from *Active Fire Data* *Earthdata* (nasa.gov), last access
152 time: 14 December 2023). The pie charts represent the chemical compositions of submicron particulate
153 matter (PM₁) along with their contributions at both sites during this campaign. The rose plots colored by
154 wind speed (WS) at (b) the YBJ site and (c) the GIG site are also shown.

155 2.2. Light absorption coefficient measurement

156 The aerosol light absorption coefficients at both sites were measured by multi-wavelength
157 Aethalometer (Model AE33, Magee Scientific Corp., Berkeley, CA, USA) at seven wavelengths (370,
158 470, 520, 590, 660, 880, 950 nm) with a high time resolution of 1 minute (Drinovec et al., 2015). Ambient
159 aerosols were introduced into AE33 through a PM_{2.5} cyclone at a flow rate of 5 L min⁻¹. The AE33
160 collected aerosols via continuous pumping to a specific location on the filter belt. It then measured the
161 transmitted light that passed through this sample-containing spot and a corresponding blank filter film
162 spot. The instantaneous light-absorbing aerosols were determined by analyzing the variation in the
163 attenuation rate of the transmitted light across the particulate-loaded filter membrane. To accurately
164 reflect the real optical absorption coefficients of airborne aerosols, a real-time compensation parameter
165 (k value) and a fixed filter multiple scattering parameter ($C_{ref} = 1.57$ for tetrafluoroethylene (TFE)-coated
166 glass filter) are required to correct the optical attenuation coefficient measured on the filter membrane.
167 For the k value, the "dual-point" measurement technique of AE33 avoids the "aerosol loading" effect
168 during single filter tape membrane sampling, enabling real-time calculation corrections for load
169 compensation parameters (Drinovec et al., 2015). Multiple studies have shown that the C value (2.8–7.8)
170 varies with different wavelengths and observation locations (Qin et al., 2018; Collaud Coen et al., 2010;
171 Tian et al., 2023; Zhang et al., 2021). In this study, the C_{final} values of 3.34 (2.23* C_{ref}) for the YBJ site
172 and 3.6 (2.3*1.57) for the GIG site were applied based on the previous studies in Tibet (Zhang et al.,
173 2021) and Guangzhou (Cai et al., 2024), also using the AE33 instrument.

174 2.3. OA measurement and source apportionment

175 The main chemical compositions of submicron aerosols including OA, nitrate, sulfate, ammonium,

176 and chloride were measured using a soot particle time-of-flight aerosol mass spectrometer (SP-AMS; 177 Aerodyne Research Inc., Billerica, MA, USA) (Onasch et al., 2012) at YBJ site and a time-of-flight 178 aerosol chemical speciation monitor (ToF-ACSM; Aerodyne Research Inc., Billerica, MA, USA) 179 (Fröhlich et al., 2013) at GIG site. During this campaign, both the SP-AMS and ToF-ACSM shared the 180 same sampling inlet with co-located AE33. The setup diagram can be found in Fig. S1. The time 181 resolution of SP-AMS and ToF-ACSM was 1 min and 40 s, respectively. For SP-AMS, dual vaporization 182 mode and tungsten-only V mode were alternatively applied every 4 minutes. In this study, tungsten-only 183 mode, which resembled the traditional HR-ToF-AMS, was applied. The ionization efficiency (IE) 184 calibration was done using monodispersed NH_4NO_3 aerosols before and after campaigns. The relative 185 ionization efficiency (RIE) of sulfate and ammonium is 1.26 and 4.24 for SP-AMS and 1.22 and 3.39 186 for ACSM, while a default RIE of 1.4 was used for OA. A constant collection efficiency (CE) of 0.5 was 187 used for YBJ measurement due to the quite low mass fraction of ammonium nitrate (< 40 %), while the 188 composition-dependent collection efficiency (average CDCE = 0.52) (Middlebrook et al., 2012) was 189 applied in GIG measurement. The SP-AMS data were processed using SQUIRREL (v1.65) and PIKA 190 (v1.25A), embedded in Igor Pro (v6.37; WaveMetrics, Inc., Lake Oswego, OR, USA), while ToF-ACSM 191 data were processed using Tofware 3.2.4 (Tofwerk AG, Thun, Switzerland).

192 The positive matrix factorization (PMF) (Ulbrich et al., 2009; Zhang et al., 2011) was applied to the 193 OA spectral matrix to resolve the sources of OA at both sites. More detailed information can be found in 194 Text S1 and Table S2. The final OA source apportionment at the YBJ site and GIG site are shown in Fig. 195 S4. At the YBJ site, five OA factors were finally resolved using free PMF with PMF3.05 (Ulbrich et al., 196 2009), including hydrocarbon-like OA (HOA, 11 %) mainly from traffic emissions, biomass burning OA 197 (BBOA, 9 %), biofuel-OA (13 %), less-oxidized oxygenated OA (LO-OOA, 42 %), and more-oxidized 198 oxygenated OA (MO-OOA, 25 %). At the GIG site, OA was resolved based on Multilinear Engine 2 199 (ME-2; SoFi 6.8) (Canonaco et al., 2013), and the standard BBOA mass spectra (Hu et al., 2016; Hu et 200 al., 2013) were introduced as an external constraint to fully constrain (a value = 0) BBOA factor at the 201 GIG site. Finally, five factors were chosen with MO-OOA (49 %) and LO-OOA (22 %) dominating the 202 total OA, followed by cooking-related OA (COA, 13 %), BBOA (8 %), and HOA (8 %).

203 2.4. Calculation of BC and BrC light absorption coefficients

204 The Absorption Ångström exponent (AAE) method was widely used to distinguish BC and BrC light 205 absorption coefficients measured by Aethalometer (Lack and Langridge, 2013). Previous studies 206 demonstrated that the aerosol light absorption at 880 nm was entirely dominated by BC (Kirchstetter et 207 al., 2004). The absorption coefficients of BrC at shorter wavelengths (370, 470, 520, 590, and 660 nm) 208 can be calculated by combining the AAE (Lack and Langridge, 2013) with BC light absorption at 880 209 nm, using the following Equations:

$$210 \quad \text{Abs}_{\text{BC}}(\lambda) = \text{Abs}(880) \times \left(\frac{880}{\lambda}\right)^{\text{AAE}_{\text{BC}}} \quad (1)$$

$$211 \quad \text{Abs}_{\text{BrC}}(\lambda) = \text{Abs}(\lambda) - \text{Abs}_{\text{BC}}(\lambda) \quad (2)$$

212 Here, $\text{Abs}_{\text{BC}}(\lambda)$ and $\text{Abs}_{\text{BrC}}(\lambda)$ (M m^{-1}) represent light absorption coefficients of BC and BrC at 213 wavelength λ (nm), respectively. $\text{Abs}(\lambda)$ represents the total aerosol light-absorbing coefficients at the

wavelength λ , which can be calculated by the mass concentration of BC ($\mu\text{g m}^{-3}$) multiplied by mass absorption cross-section (MAC; $\text{m}^2 \text{g}^{-1}$) at wavelength λ , denoted as $\text{Abs}(\lambda) = \text{BC}(\lambda) \times \text{MAC}(\lambda)$. In this study, default MAC values for BC (18.47, 14.54, 13.14, 11.58, 10.35, and $7.77 \text{ m}^2 \text{g}^{-1}$ for 370, 470, 520, 590, 660, and 880 nm, respectively) were used (Drinovec et al., 2015). AAE_{BC} denotes the wavelength dependence of pure BC particles, which was usually assumed as 1 to calculate the light absorption coefficient of BC (Tian et al., 2023; Zhang et al., 2022b). However, due to the multiple effects (e.g., lensing effect) caused by the mixing of non-BC/coating materials and BC during atmospheric evolution, the light absorption of BC can be enhanced (Jacobson, 2001; Liu et al., 2017; Peng et al., 2016). Moreover, AAE_{BC} was also found to be varied as a function of absolute wavelength values (Luo et al., 2022), which was suggested as 0.8–1.4 for BC particles (Lack and Langridge, 2013; Kasthuriarachchi et al., 2020a; Zhai et al., 2022; Corr et al., 2012). We summarized the AAE_{BC} values from the literatures in Table S3, and found all the actually used values are between 1 – 1.18. E.g., within one campaign (Kasthuriarachchi et al., 2020), 93% of directly measured AAE from ambient core BC in Singapore was found to be less than 1.1. An AAE_{BC} of 1.4 represents a typical high value, considering the mixing of non-absorbing material with BC in the extreme case (Lack and Langridge, 2013). For our study, we found ~82% of data was negative value when the AAE_{BC} of 1.4 was applied, which is unrealistic to apply here. Thus, to investigate the uncertainty of BrC estimated here, AAE_{BC} of 0.8 to 1.2 was applied, which results in 2–13 % and 4–14 % of BrC contribution to total light absorption from 370 to 660 nm for the YBJ site and GIG site, respectively.

2.5. Sources contribution to BrC light absorption based on multiple linear regression (MLR)

To further understand the sources of BrC light absorption, a multiple linear regression (MLR) was used to apportion the BrC light absorption to different components resolved by the source apportionment of OA (Kasthuriarachchi et al., 2020a; Qin et al., 2018; Tian et al., 2023; Zhang et al., 2021), using the following Equations:

$$\text{Abs}_{\text{BrC}}(\lambda) = \sum(a \times \text{Factor}) + \text{intercept} \quad (3)$$

Here, $\text{Abs}_{\text{BrC}}(\lambda)$ (M m^{-1}) represents the BrC light absorption coefficient at a wavelength of λ (370, 470, 520, 590 and 660 nm); a represent the regression coefficients of different OA components, which can be regarded as MAC ($\text{m}^2 \text{g}^{-1}$) values (Kasthuriarachchi et al., 2020a); Factor ($\mu\text{g m}^{-3}$) represents the mass concentration of OA from different sources (see Sect. 2.3).

2.5.1. Uncertainty analyses for the MLR method

Multicollinearity is an important factor leading to inaccurate estimation of regression coefficients in the MLR model. To estimate the uncertainty of the MLR method, we tested different scenarios with varied PMF factor combinations based on their correlation. To compare with other published results and simplify the calculation process, the MLR uncertainty at 370 nm was estimated. In general, four cases were chosen for the YBJ campaign, and three cases were chosen for the GIG campaign by combining or excluding collinear factors. The detailed information can be found in Text S2 and Table S5. All the cases yield similar low coefficients for the SOA factor and high coefficient values for the POA factors, suggesting the validity of MLR analysis shown here.

252 With each solution, the uncertainty of the regression coefficient (i.e., MAC) for the individual OA
 253 components input into the MLR model was evaluated using Monte Carlo simulations. For the Monte
 254 Carlo calculation input, the uncertainty of the PMF factor mass concentration needs to be evaluated. A
 255 bootstrap analysis (100 iterations; (Ulbrich et al., 2009) was applied, which shows a 9–36 % uncertainty
 256 for the PMF factors at the YBJ site and 3–9 % at the GIG site, as shown in Table S6. The uncertainty for
 257 the coefficient of BrC at 370 nm was estimated to be 43 % for the YBJ site and 36 % for the GIG site
 258 based on the lower (0.8) and upper limit of (1.2) previously reported AAE_{BC} range. The total uncertainties
 259 of each coefficient for each PMF factor were then calculated by Monte Carlo with 10,000 simulations.

260 Considering that biomass burning is widely reported as an important source of BrC light
 261 absorption and regarded as a warming agent affecting global climate (Wang et al., 2025), we
 262 consider all biomass burning related contributing sources when run the MLR model in the case of
 263 eliminating the collinearity problem in this study. As previously reported in the literature
 264 (Kasthuriarachchi et al., 2020a; Qin et al., 2018), the MAC of COA is nearly zero, thus, the light
 265 absorption by COA at GIG site was not considered in this study. We finally combined the BBOA
 266 factor and Biofuel–OA factor as BBOA (case 3) for the YBJ site and included BBOA, HOA as input
 267 (case 3) for the GIG site (Table 1). The SOA (LO–OOA and MO–OOA) at GIG site were not inputted
 268 here due to the collinearity with BBOA, the light absorption contribution and MAC values (case 3)
 269 at GIG site will be lower limits for SOA. For its upper limits, Case 2 in the supporting information
 270 (Text S2; Table S5) was also shown (Fig. S9). At the YBJ site, the MAC uncertainty of BBOA
 271 (26.4 %), HOA (20.8 %), LO–OOA (56.3 %), and MO–OOA (57.9%) was found, as shown in Table
 272 S7. For the GIG site, the MAC uncertainty of HOA (5.8 %), BBOA (6.8 %), and intercept (21.6 %)
 273 was estimated. With the final solution, the total light absorption calculated from the predicted
 274 regression coefficients (i.e., MAC) showed strong agreement with the measured values, as indicated
 275 by the slopes (YBJ: 0.9; GIG: 0.9) and Pearson correlation coefficients (YBJ: $R = 0.8$; GIG: $R =$
 276 0.7). These results suggest the robustness of the regression analyses. However, a notable intercept
 277 (0.37 M m^{-1} , representing 13 % of the total light absorption) was observed in the MLR model at the
 278 GIG site. This intercept indicates a portion of BrC light absorption that could not be explained by
 279 the OA factors, potentially due to uncertainties associated with the MLR method. The detailed
 280 discussion of MAC and BrC light absorption contributions is shown in Sect.3.2.

281 **Table 1.** Regression coefficients (MAC) of the final case of multiple linear regression (MLR) at 370, 470,
 282 520, 590, and 660 nm at the YBJ site and GIG site. Note that the SD represents the Standard deviation
 283 purely calculated from the MLR model.

| YBJ site | | | | | |
|------------------------|-----------------|-----------------|-----------------|-----------------|-----------------|
| | Wavelength (nm) | | | | |
| | 370nm | 470nm | 520nm | 590nm | 660nm |
| MAC (Average \pm SD) | | | | | |
| biofuel–OA | 1.11 ± 0.11 | 0.42 ± 0.05 | 0.11 ± 0.03 | 0.11 ± 0.02 | 0 ± 0.03 |
| HOA | 2.08 ± 0.3 | 1.11 ± 0.14 | 0.18 ± 0.10 | 0.16 ± 0.06 | 0 ± 0.07 |
| LO–OOA | 0.15 ± 0.08 | 0.14 ± 0.03 | 0.07 ± 0.02 | 0.04 ± 0.02 | 0.01 ± 0.02 |
| MO–OOA | 0.18 ± 0.18 | 0.19 ± 0.08 | 0 ± 0.06 | 0.02 ± 0.04 | 0 ± 0.04 |
| Intercept | 0 ± 0.02 | 0.02 ± 0.01 | 0.04 ± 0.01 | 0.02 ± 0 | 0.03 ± 0 |
| GIG site | | | | | |
| | Wavelength (nm) | | | | |
| | 370nm | 470nm | 520nm | 590nm | 660nm |
| MAC (Average \pm SD) | | | | | |
| BBOA | 1.91 ± 0.21 | 0.90 ± 0.10 | 0.35 ± 0.06 | 0.40 ± 0.04 | 0.20 ± 0.02 |
| HOA | 2.57 ± 0.28 | 1.40 ± 0.13 | 0.72 ± 0.07 | 0.38 ± 0.06 | 0.13 ± 0.03 |

| | | | | | |
|-----------|-----------------|-----------------|-----------------|-----------------|-----------------|
| Intercept | 0.37 ± 0.17 | 0.18 ± 0.08 | 0.42 ± 0.04 | 0.17 ± 0.03 | 0.11 ± 0.02 |
|-----------|-----------------|-----------------|-----------------|-----------------|-----------------|

284 **2.6. Calculation of radiative forcing**

285 The estimation of the direct radiative forcing caused by BrC was conducted using a model known
 286 as the “simple forcing efficiency (SFE)”, which can provide a radiative forcing (W g^{-1}) based on a given
 287 mass of aerosols. Although the resulting value of SFE is lower than that projected by climate models, it
 288 still serves as a valuable tool for gauging the sensitivity of various input parameters (Bond et al., 2006;
 289 Chylek and Wong, 1995). In this study, we used a modified version of the wavelength-dependent SFE
 290 without considering mass scattering and expressed it as follows (Tian et al., 2023; Zhang et al., 2020a;
 291 Zhang et al., 2022b):

292
$$SFE(\lambda) = \frac{S(\lambda)}{4} \times \tau_{atm}^2 \times (1 - F_c) \times 4\alpha_s \times MAC(\lambda) \quad (4)$$

293 Here, $S(\lambda)$ ($\text{W g}^{-1} \text{nm}^{-1}$) is the wavelength-dependent solar irradiance based on the ASTM G173–
 294 03 Reference Spectra (<https://www.nrel.gov/grid/solarresource/spectra-am1.5.html>); τ_{atm} represents
 295 atmospheric transmission (0.79); F_c is the cloud fraction (0.6); α_s is the surface albedo (global average
 296 0.19) (Chen and Bond, 2010). $MAC(\lambda)$ ($\text{m}^2 \text{g}^{-1}$) is the mass absorption cross-section of different OA
 297 components at wavelength λ at a 1 nm resolution. The $MAC(\lambda)$ can be calculated according to the
 298 power–law fitting results between the MAC from each OA component at different wavelengths (370 to
 299 660 nm) in this study. Note that the SFE represents a straightforward calculation designed to ascertain
 300 the relative significance of diverse optical properties of radiative forcing. However, to accurately
 301 determine forcing efficiency, a comprehensive radiative transfer model is still necessary (Efremenko and
 302 Kokhanovsky, 2021).

303 **3. Results and discussion**

304 **3.1. Overview of Aerosol light absorption**

305 The summarized total aerosol light absorption coefficients (Abs_{total}) as a function of wavelength at
 306 two sites are shown in Fig. 2 and Table S8. The more detailed temporal evolutions of Abs_{total} at two
 307 sites are displayed in Fig. S7. In general, the average Abs_{total} ranged from 0.6 to 1.6 M m^{-1} (370 to 950
 308 nm) at the YBJ site, while the 7–8 times higher Abs_{total} ($4.2\text{--}13.2 \text{ M m}^{-1}$) was observed at the GIG site
 309 (Fig. 2a and Table S8). This discrepancy was primarily attributed to the much higher aerosol mass
 310 concentration in urban Guangzhou ($\text{PM}_1: 12.5 \pm 8.8 \mu\text{g m}^{-3}$) compared to the background Tibetan region
 311 ($\text{PM}_1: 1.0 \pm 0.6 \mu\text{g m}^{-3}$) (Figs. 2a and 2b). The campaign-averaged BrC light absorption coefficients
 312 (Abs_{BrC}) and its contribution to total aerosol light absorption increased with decreasing wavelength at
 313 both sites (AAE of BrC is 2.6 for YBJ and 3.2 for GIG; Figs. 2c, 3b, and 3d), indicating strong BrC light
 314 absorption at shorter wavelengths. At 370 nm, where BrC contributes the most to the total light absorption,
 315 Abs_{BrC} in Tibet ($0.2 \pm 0.3 \text{ M m}^{-1}$) was found to be a factor of 13 lower than that in Guangzhou (2.9 ± 2
 316 M m^{-1}). This finding is consistent with the much lower OA mass concentrations (by a factor of ∼10) at
 317 the YBJ site (OA: $0.7 \pm 0.4 \mu\text{g m}^{-3}$ vs $6.9 \pm 5.8 \mu\text{g m}^{-3}$ at GIG; Figs. 2b and 2c).. A positive correlation
 318 between BrC light absorption and OA mass concentration was also observed across different field studies
 319 (Fig. 2d; Table S4). This relationship aligns with the findings of Wang et al. (2022a), who reported that

320 BrC light absorption at 365 nm positively correlates with OA mass concentration across various sources.

321 To facilitate a visual comparison with previous studies, the literature-reported BrC light absorption
322 results at 365 or 370 nm are summarized in Fig. 3e and Table S4. This wavelength was chosen due to its
323 higher BrC abundance across different wavelengths, which leads to less uncertainty. At the YBJ site, the
324 campaign-averaged Abs_{BrC} at 370 nm (0.2 M m^{-1} ; $0.03\text{--}0.6 \text{ M m}^{-1}$ for 5–95 % range; Table S4) was
325 lower than the values reported across the Qinghai–Tibet Plateau (QTP) ($0.6\text{--}14.9 \text{ M m}^{-1}$), e.g., the BrC
326 light absorption at YBJ site (central QTP) was much lower than those observed at the edges of the QTP,
327 such as Ngari ($5.9\text{--}10.7 \text{ M m}^{-1}$), Qomolangma Station (QOMS, 4.4 M m^{-1}), and Gaomeigu (12.3 M m^{-1}),
328 where elevated values are primarily influenced by the cross–border transport of biomass burning
329 plumes during pre–monsoon or post–monsoon period (Zhang et al., 2021; Tian et al., 2023; Zhu et al.,
330 2017). The low BrC light absorption at YBJ can be attributed to the extremely low mass loading of OA
331 ($0.7 \pm 0.5 \text{ } \mu\text{g m}^{-3}$), which is influenced by wet deposition from precipitation and specific atmospheric
332 circulation patterns during July, a monsoon period (Xu et al., 2018; Zhao et al., 2013). In addition, the
333 absolute BrC light absorption coefficient at YBJ was comparable to levels measured in certain remote
334 regions, such as the Arctic ($0.04\text{--}0.2 \text{ M m}^{-1}$ at 365 nm) (Barrett and Sheesley, 2017; Yue et al., 2022; Yue
335 et al., 2019), highlighting the relatively clean atmospheric conditions at YBJ as a background site in Tibet.
336 In general, BrC light absorption in urban areas tends to be higher or comparable to that in QTP regions
337 due to typically higher OA mass concentrations (Fig. 2d).

338 Although a relatively large discrepancy in the absolute light absorption coefficient of BrC was
339 observed between the YBJ and GIG sites, the contribution of BrC to total aerosols ($\text{Fraction}_{\text{BrC}}$) was
340 comparable at both sites (15 % vs. 21 %), highlighting the significant role of BrC in light absorption at
341 both locations. We summarized $\text{Fraction}_{\text{BrC}}$ across different studies and regions, as shown in Fig. 3e and
342 Table S4, which reveals that $\text{Fraction}_{\text{BrC}}$ values generally fall within a range of 8–58 %. Notably, the
343 $\text{Fraction}_{\text{BrC}}$ in the Qinghai–Tibet Plateau (QTP) is comparable to that in urban areas. Furthermore, a clear
344 trend shows that $\text{Fraction}_{\text{BrC}}$ at the edges of the northeastern (such as Qinghaihu Lake) and south QTP
345 (such as Ngari) tends to be higher than in the central QTP (such as Beiluhe, Namco, and YBJ site), and
346 the $\text{Fraction}_{\text{BrC}}$ in Northern China is generally higher than in Southern China. To better understand the
347 factors driving the $\text{Fraction}_{\text{BrC}}$, we investigated the relationship between the contribution of primary
348 organic aerosol (POA) and secondary OA (SOA) to total OA and the $\text{Fraction}_{\text{BrC}}$. As illustrated in the
349 inset plot of Fig. 3e, a positive correlation was observed, suggesting that the enhanced POA contribution
350 will increase the BrC light absorption contribution in carbonaceous aerosol. For sites at the edges of the
351 QTP and in northern Chinese cities, where the $\text{Fraction}_{\text{BrC}}$ is higher, OA is significantly influenced by the
352 combustion of solid fuels, including coal and biomass, particularly during winter. This finding signifies
353 the importance of POA in contributing to ambient BrC light absorption.

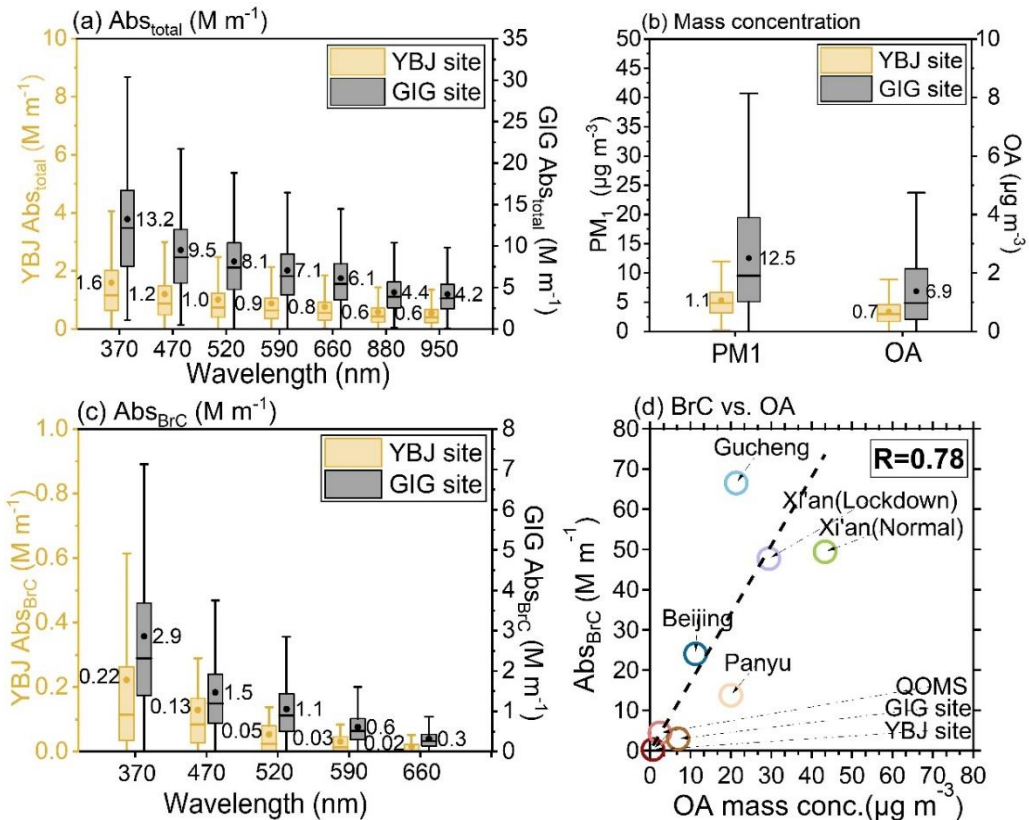
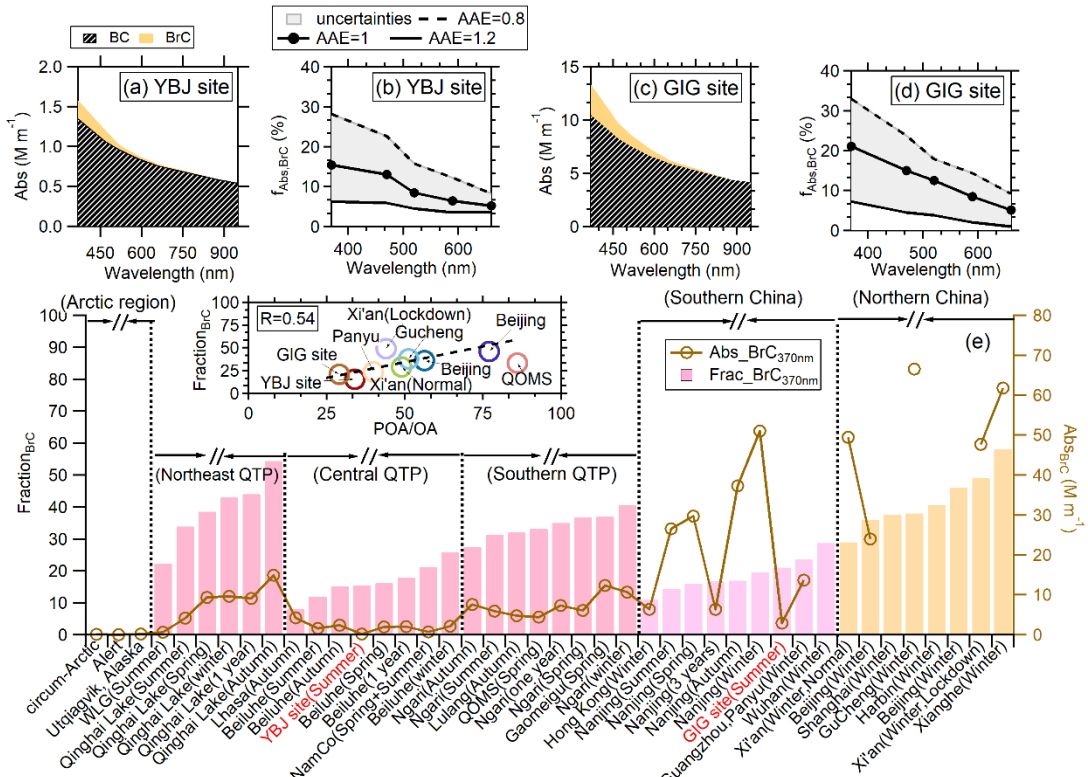
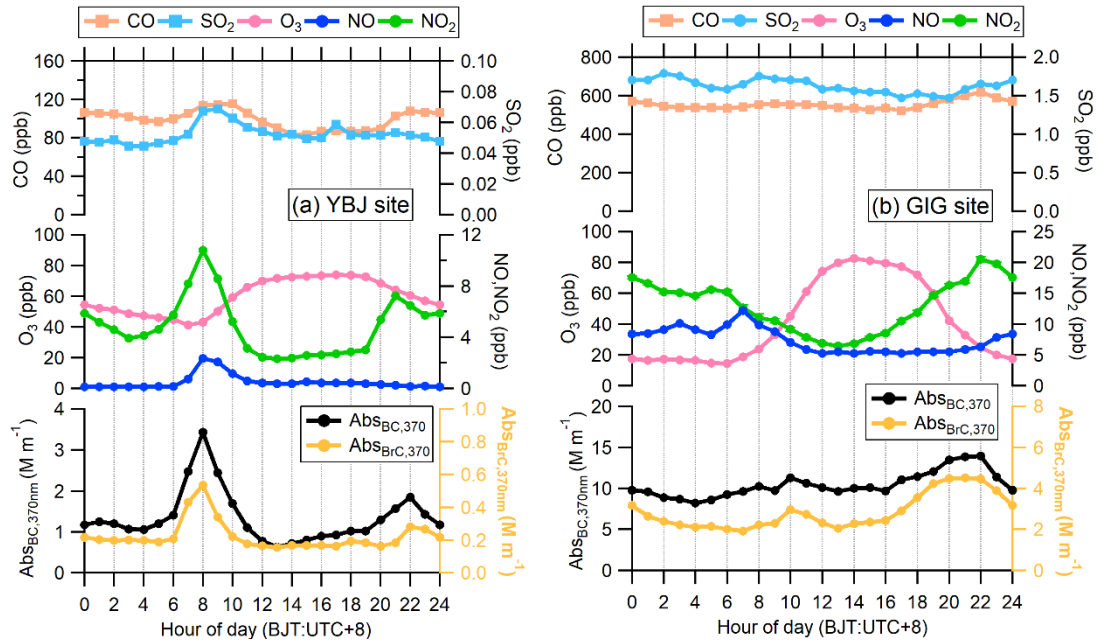


Figure 2. Box plot of the light absorption coefficient of total aerosols (Abs_{total}) (a) and BrC (Abs_{BrC}) (c) from 370nm to 950nm at YBJ (left Y axis) and GIG (right Y axis) sites. The Abs_{BrC} was separated from the Abs_{total} based on Eq. (1) and (2) using $AAE_{BC}=1$, (b) Box plot of PM_1 and OA mass concentrations at the YBJ site and GIG site. The whiskers indicate the 90th and 10th percentiles, the upper and lower boundaries of boxes indicate the 75th and 25th percentiles, the lines in the boxes indicate the median values, and the markers for the mean values. (d) Scatter plot of the BrC absorption coefficient as a function of OA concentration (data from the literature (Table S3)).



363 Figure 3. The absolute light absorption coefficients of BC (Abs_{BC}) and BrC (Abs_{BrC}) at wavelengths from
 364 370 to 880 nm at the (a) YBJ site and (c) GIG site, respectively. The BrC was calculated based on the
 365 AAE of BC (AAE_{BC})=1. The contribution of BrC light absorption at wavelengths from 370 to 660 nm at
 366 the (b) YBJ site and (d) GIG site, respectively. The grey-filled area represents variations in the BrC light
 367 absorption fraction caused by the AAE_{BC} from 0.8 (dashed line) to 1.2 (solid line). The circle makers are
 368 the average value estimated based on AAE_{BC}=1. (e) The summary of BrC light absorption coefficients
 369 (the brown circles) and their contributions to total light absorption coefficients at 370 nm from the
 370 literature results. The results were categorized according to the locations of their observation sites (Arctic
 371 region, Qinghai-Tibet Plateau (QTP region), Southern China, and Northern China). The inset plot
 372 represents the relationship between the BrC light absorption fraction and the contribution of primary OA
 373 to total OA. The detailed information is provided in Table S4.

374 To further elucidate the dynamic evolution of BrC light absorption, the diurnal variations of
 375 $Abs_{BC,370}$ and $Abs_{BrC,370}$ were displayed in Fig. 4 (Abs_{total} at different wavelengths was shown in Fig. S8).
 376 $Abs_{BC,370}$ and $Abs_{BrC,370}$ at both sites peaked simultaneously, indicating combustion source for BC are
 377 also important contributor to the BrC in both studies. At the YBJ site, the peaks at 08:00 and 22:00 align
 378 with the NO_x (NO + NO₂) and CO, which were due to the local or regional anthropogenic emissions
 379 (such as vehicle emissions and other combustion activities) in Tibet. In other periods, a background
 380 $Abs_{BrC,370}$ value of 0.19 M m⁻¹ was found at YBJ site. The diurnal patterns of $Abs_{BC,370}$ and $Abs_{BrC,370}$
 381 at the GIG site, which showed an enhancement at 10:00 and a stronger peak at 21:00, were slightly
 382 different from those at the YBJ site. This difference suggests distinct source emissions or secondary
 383 formation patterns between the two locations (Fig. 4b and Fig. S8b). Higher increase of NO₂/NO and CO
 384 at night in Guangzhou was also found, implying the potentially important contribution of vehicles and
 385 other combustion sources, e.g., biomass burning, at this urban site.



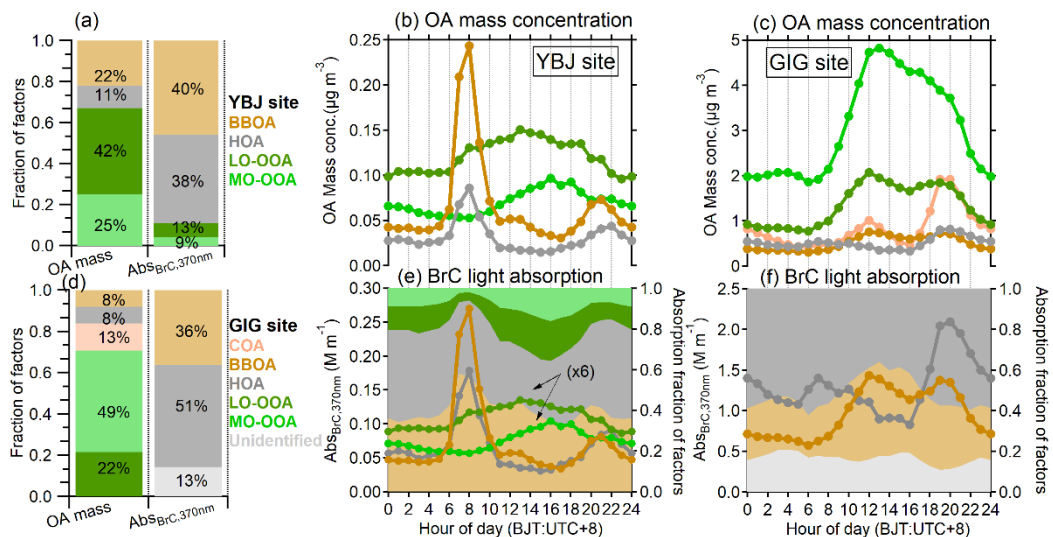
386
 387 Figure 4. Diurnal variations of gas pollutants and BC/BrC light absorptions at 370 nm at (a) YBJ site and
 388 (b) GIG site.

389 3.2. Optical properties of source-specific BrC

390 To further identify the source of absorptive BrC in this study, we applied the multiple linear
 391 regression (MLR) method to attribute BrC light absorption at different wavelengths to OA components
 392 from various sources, based on the PMF analysis conducted at the YBJ and GIG sites. The detailed

393 methodology is described in Sect.2.5.

394 At the YBJ site in Tibet, the MLR model identified BBOA (the sum of BBOA and Biofuel–OA, as
 395 defined in Sect.2.5.1 and Text S1), HOA, LO–OOA, and MO–OOA as the main contributors to BrC light
 396 absorption. As shown in Fig. 5a, secondary organic aerosol (SOA, comprising LO–OOA and MO–OOA)
 397 dominated the total OA mass concentration (67 %), followed by BBOA (22 %) and HOA (11 %).
 398 However, for BrC light absorption, POA (including BBOA and HOA) emerged as the most significant
 399 contributor, with BBOA contributing the most (40 %), followed by HOA (38 %) and SOA (22 %),
 400 signifying the key role played by biomass burning and vehicle emissions for BrC light absorption at the
 401 YBJ site. Indeed, both the BBOA ($R = 0.77$) and HOA ($R = 0.64$) show better correlations with BrC light
 402 absorption at 370 nm than other factors (Fig. S10). A similar trend was observed at the GIG site in urban
 403 Guangzhou (Fig. 5d), where POA (including BBOA, HOA) represented only 29 % of the total OA mass
 404 concentration but contributed disproportionately to BrC light absorption (89 %). These findings highlight
 405 the critical role of primary BrC in light absorption during our measurement campaign. In the following,
 406 we will discuss each source contribution to BrC in detail.



407
 408 Figure 5. (a) The contributions of different OA factors to total OA (left bars) and contributions of different
 409 OA factors to BrC light absorption at 370 nm (right bars) at the YBJ site and GIG site. The diurnal
 410 variations of OA factors mass loading and the light absorption of different OA components at 370 nm at
 411 the YBJ site (b, e) and GIG site (c, d). The “x6” indicates the light absorption of LO-OOA and MO-OOA
 412 at 370 nm expanded by 6 times to better guide the eyes for the trend of diurnal patterns.

413 3.2.1. Optical properties of BBOA

414 The diurnal variations of the biomass burning OA (BBOA) light-absorbing coefficients at 370 nm
 415 for the YBJ site exhibited strong correlation with BBOA mass concentration (Fig. 5b, 5e), characterized
 416 by distinct peaks at 08:00 and 21:00 local time. This temporal pattern aligns with the observation reported
 417 in urban Lhasa, which exhibits a peak at 9:00 and 22:00, respectively (Zhao et al., 2022). The BBOA
 418 peaks at the YBJ site (central QTP) in the morning and night are primarily influenced by local
 419 anthropogenic activities, i.e., the traditional Weisang ritual. The Weisang activity, prevalent throughout
 420 Tibet, including the sparsely populated YBJ region, typically occurs twice daily in the morning and
 421 evening. Wherever Tibetans are living, almost all have a Weisang furnace. This cultural practice involves
 422 the combustion of specific organic materials, including wormwood, cypress branches, highland barley,

423 ghee lamp, and zanba in dedicated stoves, generating characteristic mulberry smoke for religious
424 purposes (Zhang et al., 2020b; Zhang et al., 2022a). Additionally, traditional residential solid biofuel
425 combustion (primarily yak dung and wood) for cooking and space heating contributes significantly to
426 BBOA loading in the plumes (Shen et al., 2021). The AMS spectral similarity between ambient BBOA
427 and emissions from both Weisang activities and solid biofuel combustion (Zhang et al., 2022a), showing
428 the highest signals of m/z 41, 43 and 55, and high abundance of hydrocarbon ions above m/z 60, provides
429 further evidence for their dominant contributions to regional BBOA in Tibet. The hourly wind roses show
430 that the wind direction at the YBJ site exhibits a regular diurnal pattern, with a gradual change from the
431 north wind in the morning to the stronger southeast wind in the afternoon (Fig. S11). Combining the
432 Bivariate polar plots, the higher morning peak (6:00 to 11:00) of BBOA was from the nearby residential
433 area under low wind speed condition (Figs. S12, 13), while the lower evening peak was due to the dilution
434 of stronger wind speed in the evening (17:00 to 24:00) (Figs. S12, 13).

435 Compared to Tibet, the urban Guangzhou exhibited fundamentally different diurnal patterns in both
436 BBOA mass concentration and BrC light absorption coefficients (Fig. 5c, 5f), where the BBOA peak
437 occurs around noon and nighttime, reflecting the different biomass burning activity between Tibet and
438 Guangzhou. Previous literature (Cai et al., 2023; Wang et al., 2017) reported that the agriculture burning
439 at the suburban areas likely dominated the BBOA mass concentration at Guangzhou areas.

440 The mass absorption coefficient (MAC, $\text{m}^2 \text{ g}^{-1}$), a crucial optical parameter for BrC characterization,
441 quantifies the light absorption capacity per unit mass of OA. Our measured MAC values for BBOA
442 ($1.11\text{--}2.54 \text{ m}^2 \text{ g}^{-1}$ at YBJ vs. $1.91 \pm 0.21 \text{ m}^2 \text{ g}^{-1}$ at GIG; Table 1, S4) fall within the lower range of
443 previously reported values ($0.6\text{--}8 \text{ m}^2 \text{ g}^{-1}$; Fig. 6, Table S10). This variability in MAC values from similar
444 combustion sources, as documented in numerous studies (Budisulistiorini et al., 2017; Chen and Bond,
445 2010; Martinsson et al., 2015; Saleh et al., 2014), arises from multiple factors, including fuel composition,
446 combustion conditions, and efficiency. The relatively low MAC values observed at both sites in this study
447 can be attributed to several reasons: 1) Both studies were conducted in the summer time, which coincided
448 with intense solar radiation and elevated oxidant concentrations, promoting photobleaching of
449 chromophores in fresh BBOA (Sumlin et al., 2017). Recent experimental evidence (Hems et al., 2021)
450 demonstrates rapid (minutes to hours), nonlinear photobleaching kinetics of fresh BrC, highlighting the
451 complex nature of these atmospheric processes. Especially for the Guangzhou samples, BBOA from
452 regional transport was likely subjected to a longer oxidation process, which led to a lower MAC at the
453 GIG site. 2) Combustion conditions and fuel type significantly influence MAC values (Martinsson et al.,
454 2015). Zhang et al. (2022a) systematically characterized Tibetan biofuel emissions, revealing that
455 Weisang materials and yak dung produce abundant OA with relatively low light absorption efficiency
456 due to incomplete combustion. Similarly, Moschos et al. (2024) showed higher MAC values for
457 hardwoods ($0.8\text{--}1.6 \text{ m}^2 \text{ g}^{-1}$) versus animal dung ($0.2\text{--}0.7 \text{ m}^2 \text{ g}^{-1}$); 3) At YBJ site, the multiple linear
458 regression (MLR) model incorporates biofuel–OA, which contains cooking OA, typically characterized
459 by weak/no absorption (Kasthuriarachchi et al., 2020a; Qin et al., 2018). The spectral similarity between
460 COA and biofuel–OA prevents complete separation in PMF analyses. Sensitivity analyses (Sect.2.5.1
461 and Text S1; Table S5) demonstrate MAC_{BBOA} variability ($1.11\text{--}2.54 \text{ m}^2 \text{ g}^{-1}$) under different model
462 assumptions, with maximum values ($2.54 \text{ m}^2 \text{ g}^{-1}$) obtained when excluding biofuel–OA contributions.

463 3.2.2. Optical properties of HOA

464 The light-absorbing coefficient of HOA at the YBJ site exhibited a pronounced peak at 08:00 and a
465 minor peak at 22:00 (Fig. 5b, 5e), aligning with the diurnal variation of HOA mass concentration. In the
466 Tibetan Plateau region, heavy-duty diesel trucks, which are critical for transporting essential goods
467 across this remote area, constitute a significant emission source alongside gasoline vehicles (Liu et al.,
468 2021; Xiang et al., 2024). Our observation site is located less than 1 km (straight-line distance) from the
469 G6 Beijing–Tibet Expressway. The Bivariate polar plots also show that the HOA was affected by the
470 wind direction, with the morning peak affected by the north and northeast plumes, while the evening
471 peak was affected by the southeast and northeast plumes with stronger wind speed. The traffic emission
472 during the night is more regional than that in the morning, which was supported by the fact that the NO
473 mass concentration was only enhanced during the morning (2.3 ppb) but not during the night, while an
474 obvious NO₂ peak at both periods (10 ppb and 7.2 ppb) was observed (Fig. 4a). Combining the Rose
475 plots and Bivariate polar plots (Fig. S12), the evening peak of HOA was also affected by the
476 southeast and northeast traffic emissions plumes with stronger wind speed, which also supported
477 the regional nature of evening HOA peak. At the urban GIG site in Guangzhou, HOA light absorption
478 coefficients displayed a bimodal distribution with a moderate morning peak at 07:00 and a stronger
479 evening peak at 20:00 (Figs. 5c, 5f), consistent with typical urban traffic emissions for rush hours (Chen
480 et al., 2021). The much higher evening peak than the morning peak coincides with rush-hour traffic
481 congestion, suggesting intensified vehicular emissions during these periods, as well as the effects of
482 meteorological conditions (e.g., reduced boundary layer height). The different diurnal variation of light
483 absorption on both HOA and BBOA between Tibetan and Guangzhou observations highlights the
484 regionally specific emission drivers from different areas.

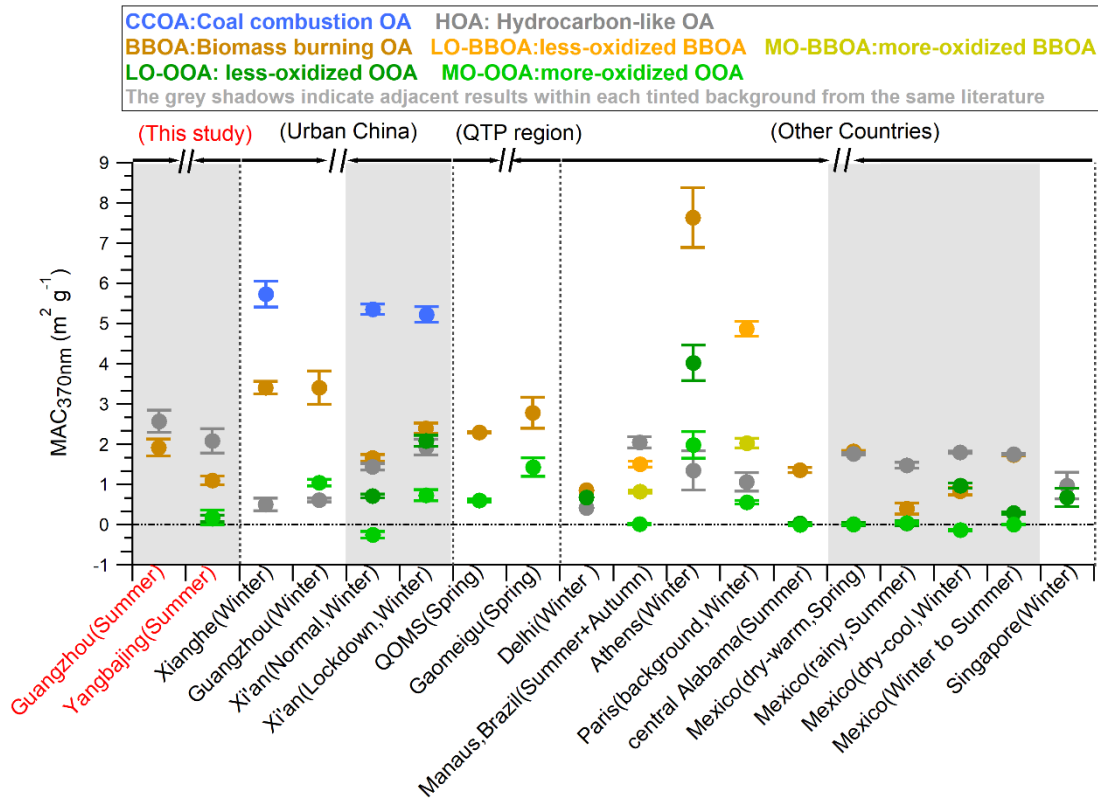
485 In our study, the MAC of HOA for Tibet ($2.08 \pm 0.3 \text{ m}^2 \text{ g}^{-1}$) and urban Guangzhou ($2.57 \pm 0.28 \text{ m}^2$
486 g^{-1}) (Table 1) were in the higher ranges of HOA MAC values reported by other studies ($0.4\text{--}2.04 \text{ m}^2 \text{ g}^{-1}$)
487 (Table S10). Note that since the OOA factors in Guangzhou were not considered in the BrC source
488 apportionment due to collinearity with BBOA, the HOA reported here shall be an upper limit. The results
489 of both observation sites show that the HOA MAC ($2.08 \text{ m}^2 \text{ g}^{-1}$ at YBJ site vs. $2.57 \text{ m}^2 \text{ g}^{-1}$ at GIG site)
490 is larger than the BBOA MAC ($1.11\text{--}2.54 \text{ m}^2 \text{ g}^{-1}$ at YBJ vs. $1.91 \pm 0.21 \text{ m}^2 \text{ g}^{-1}$ at GIG). To investigate
491 whether the MAC from ambient BBOA or HOA is higher, we summarized the MAC results from different
492 field studies in Fig. 6, yet no clear conclusion can be drawn. E.g., Higher HOA MAC than BBOA was
493 observed for central Amazon study (De Sá et al., 2019) and Mexico study (Retama et al., 2022), while
494 much higher BBOA MAC than HOA was found for Xianghe, Athens, Paris studies (Kaskaoutis et al.,
495 2021; Wang et al., 2019b; Zhang et al., 2020c). For emission experiments, higher MAC for diesel exhaust
496 than crop and wood have also been observed (Cheng et al., 2011; Du et al., 2014). In addition, very strong
497 light absorption capacity (MAC; $5\text{--}6 \text{ m}^2 \text{ g}^{-1}$) (Table S10) induced by coal combustion (Wang et al., 2019b;
498 Zhang et al., 2022b) was found, which is comparable to these extreme MAC values reported from
499 biomass burning ($5\text{--}7.5 \text{ m}^2 \text{ g}^{-1}$) (Table S10) (Kaskaoutis et al., 2021; Zhang et al., 2020c). The diversity
500 of MAC from different combustion sources implies the complex influences on light absorption from
501 multiple factors, e.g., ambient oxidation, combustion efficiency and fuel types. The comparable and

502 diverse MAC between HOA and BBOA (Cappa et al., 2019; Zhong and Jang, 2014) warrants reevaluation
503 of traffic aerosols' climate forcing and the necessity for clarifying MAC parameterizations for different
504 sources.

505 **3.2.3. Optical properties of SOA**

506 Compared with the diurnal variation characteristics of BBOA and HOA from local emissions at YBJ
507 site, light absorption coefficients of the less-oxidized oxygenated OA (LO-OOA) and more-oxidized
508 oxygenated factor (MO-OOA) were characterized by high values during the day and low values at night
509 (Fig. 5b, 5e). This day-enhanced temporal variation aligns with that of MO-OOA reported at NamCo
510 (an observation station in central QTP) (Xu et al., 2018), which is influenced by the enhanced secondary
511 BrC from photochemical oxidation during the day. In this study, the contribution of LO-OOA factor
512 shows a broad increase to $Abs_{BrC,370nm}$ during the day and peaks around 14:00 (20 %), while MO-OOA
513 contribution (16 %) peaks approximately two hours later (16:00). The different diurnal variation of MO-
514 OOA and LO-OOA suggests different formation pathways. In general, LO-OOA is characterized by
515 freshly formed SOA showing a higher light absorption contribution (13 %) than that of MO-OOA (9 %),
516 which more represents the regionally aging SOA (Figs. 5b, 5e). For the GIG site, the maximum direct
517 light absorption contribution from SOA incorporated into case 2 (see Sect.2.5.1 and Text S1; Tables S4
518 and S6) is 33 % (Fig. S9).

519 The MAC of SOA (LO-OOA and MO-OOA) showed much lower values (0.15 and 0.18 $m^2 g^{-1}$;
520 Table 1, Fig. 6) than primary sources (e.g., BBOA and HOA), consistent with their higher degree of
521 oxidation leading to the weaker light absorptivity of OA (Lee et al., 2014; Lambe et al., 2013). Lower
522 MAC of SOA ($0\text{--}4 m^2 g^{-1}$) (Table S10) than POA ($0.4\text{--}8 m^2 g^{-1}$) has also been observed in multiple other
523 ambient (De Sá et al., 2019; Retama et al., 2022; Tian et al., 2023; Washenfelder et al., 2015; Zhang et
524 al., 2021; Zhang et al., 2022b) and laboratory studies (Ni et al., 2021; Hems et al., 2021; Zhong and Jang,
525 2014).



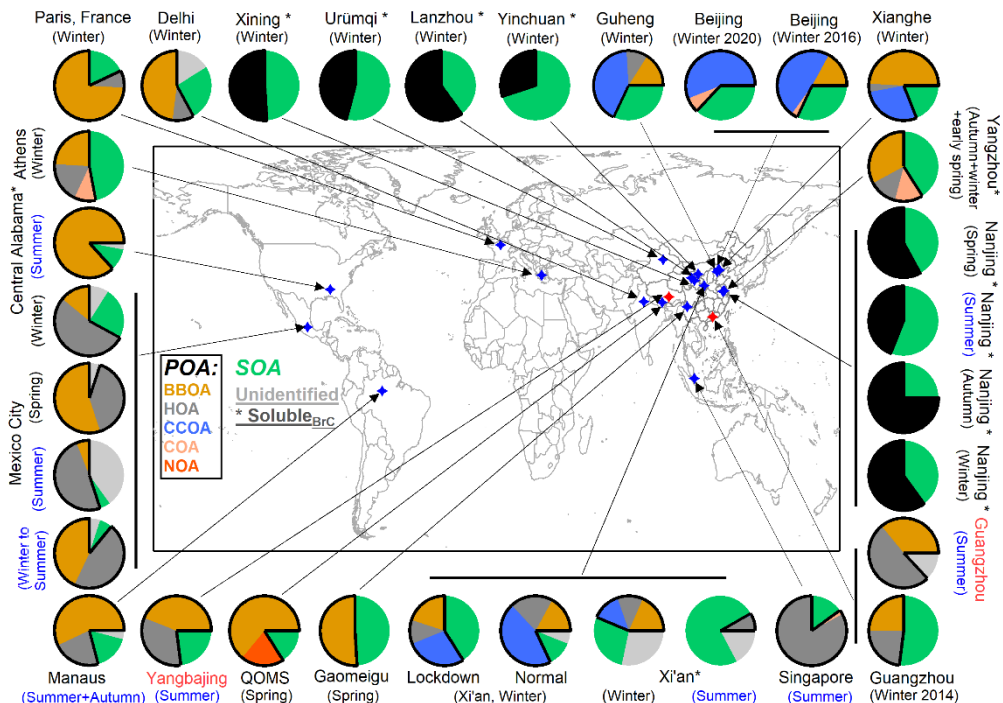
526

527 Figure 6. The literature summary of MAC from different BrC sources, which was obtained by the PMF–
 528 MLR method in different environments. All the results were categorized based on the locations of their
 529 observation sites (urban China, Qinghai–Tibet Plateau (QTP region), and other countries). Note the MO–
 530 OOA in Paris study represents OOA. Shadows indicate adjacent results within each tinted background
 531 from the same literature. The detailed information is provided in Table S10.

532 3.2.4. Summarized source contribution to BrC in the field studies

533 Figs. 7 (detailed data in Table S9) summarizes the light absorption contributions of OA from various
 534 sources across different regions, based on PMF and MLR analyses. Offline filter results are denoted by
 535 an asterisk in the pie chart. Based on this dataset, several features were found: 1) POA (primary organic
 536 aerosol) significantly influence ambient BrC light absorption on a global scale, accounting for 30–95 %
 537 of the BrC light absorption except the extremely low fraction (8.3 %) in Xi'an during summer (Lei et al.,
 538 2019). In particular, 3 quarters of the summarized study (based on number, as shown in Fig. S14) show
 539 that the POA contributes more than 50 % of BrC light absorption, signifying the important contribution
 540 of primary emission to total BrC. In the recent global model, Li et al. (2025) also found the primary
 541 emission dominated (77 %) the total light absorption from Nitrogen compounds. Note that the offline
 542 studies may underestimate the light absorption contribution of POA due to the application of soluble BrC
 543 (Bao et al., 2022; Chen et al., 2020; Lei et al., 2019; Zhong et al., 2023); 2) Key POA sources of BrC
 544 light absorption include coal combustion, biomass burning, and traffic emissions, with their light
 545 absorption contributions relative to total OA of 1–56 % (average: 33 %), 6–85 % (average: 38 %) and 4–
 546 83 % (average: 27 %), respectively (Fig. 7 and Table S9); 3) Coal combustion is especially evident in
 547 northern China during winter, with light absorption contribution of 30–89 % relative to POA (Lei et al.,
 548 2019; Sun et al., 2021; Wang et al., 2019b; Zhang et al., 2022b). In areas not subject to coal combustion,
 549 the biomass burning and traffic emissions dominate primary BrC light absorption, which can contribute

550 11–100 % (53 % for average) and 5–98 % (43 % for average) of primary BrC, respectively (Retama et
 551 al., 2022; De Sá et al., 2019; Kaskaoutis et al., 2021; Kasthuriarachchi et al., 2020a; Singh et al., 2021;
 552 Washenfelder et al., 2015; Zhang et al., 2020c). 4) The light absorption contribution from different
 553 sources showed significant spatial and temporal differences, e.g., HOA shows extremely high light
 554 absorption contribution in Singapore during summer (83 %), and in Mexico in both winter (54 %) and
 555 summer (49 %), while biomass burning dominated in central Alabama (85 %) and Paris (74 %). Given
 556 the pronounced spatial and temporal variations in source–specific light absorption, it is essential to
 557 conduct region–specific and season–specific observational research for a better understanding of the BrC
 558 sources and to better understand BrC sources and to better validate model simulations.



559
 560 Figure 7. The summary of the contribution to BrC light absorption at 370 nm from different sources using
 561 the PMF–MLR method. The asterisks (*) represent the light absorption contributions of soluble BrC
 562 from different sources at 365nm. The sources include POA: biomass burning OA (BBOA), hydrocarbon–
 563 like OA (HOA), coal combustion OA(CCOA), cooking–related OA(COA), nitrogen-containing
 564 OA(NOA); The total SOA from oxygenated OA was used here. In addition, the unidentified fraction
 565 from the intercept of the MLR method was also shown. The detailed information on each pie is provided
 566 in Table S9.

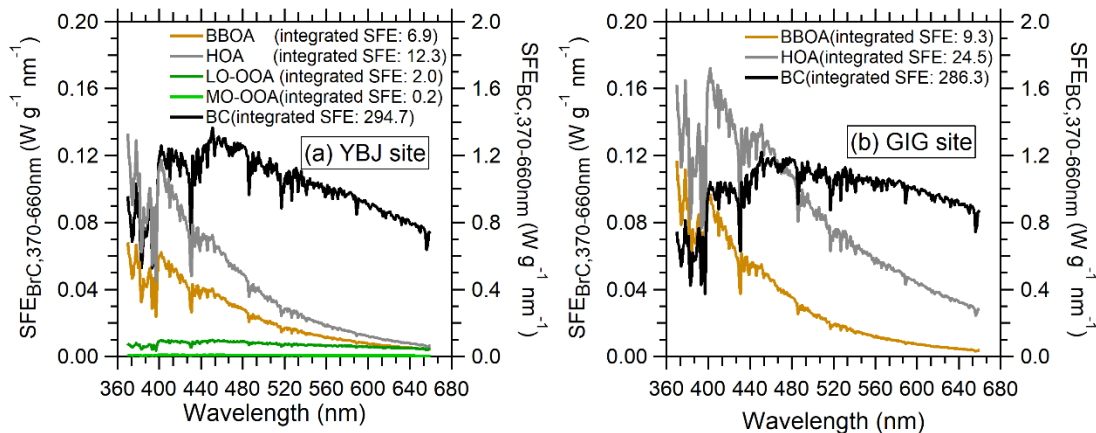
567 3.3. Radiative effect of BrC from different sources

568 The simple forcing efficiency (SFE) of different organic aerosol (OA) components at the YBJ and
 569 GIG sites was estimated using Eq. (4) as described in Sect.2.6. This methodology has been widely applied
 570 to evaluate the climate impact of brown carbon (BrC) (Tian et al., 2023; Wang et al., 2019b; Zhang et al.,
 571 2022b; Zhong et al., 2023). As illustrated in Fig. 8, black carbon (BC) emerged as the dominant light–
 572 absorbing component, exhibiting the highest integrated SFE values of 294.7 W g^{-1} at the YBJ site and
 573 286.3 W g^{-1} at the GIG site. In contrast, the integrated total SFE (from total OA absorption) across the
 574 370–660 nm wavelength range was 21.4 W g^{-1} at the YBJ site and 33.8 W g^{-1} at the GIG site, representing
 575 approximately 9–13 % of the BC values. This is consistent with the well–documented strong light–
 576 absorbing properties of BC (Gustafsson and Ramanathan, 2016), while also highlighting the significant

577 role of BrC in short-term climate effects.

578 The SFE values for POA at the YBJ (19.2 W g^{-1}) and GIG (33.8 W g^{-1}) sites were comparable to
 579 those observed in other urban areas, such as Xi'an (approximately 33 W g^{-1} for HOA + BBOA + CCOA)
 580 during winter (Zhang et al., 2022b). POA, including BBOA and HOA, contributed significantly to the
 581 total BrC light absorption, accounting for over 80 % of the BrC-specific SFE in this study. These findings
 582 underscore the substantial influence of anthropogenic emissions on aerosol radiative forcing and their
 583 implications for regional and global climate systems.

584 From an environmental and climatic perspective, these results emphasize the critical role of both
 585 BC and BrC in modulating atmospheric radiative balance. The higher SFE of BC underscores its potent
 586 warming effect, while the non-negligible contribution of BrC, particularly from POA, highlights the
 587 importance of addressing anthropogenic sources. Further elucidating the fossil and non-fossil
 588 contribution, i.e., vehicle emission, coal vs. biomass burning combustion to the BrC, is vital for refining
 589 climate models, informing mitigation strategies, and developing policies aimed at reducing short-lived
 590 climate pollutants to mitigate near-term climate change and its associated environmental impacts.



591
 592 Figure 8. The Simple forcing efficiency (SFE) of BrC from different sources and BC from 370 to 660
 593 nm at (a) YBJ and (b) GIG site.

594 4. Conclusions

595 To explore the optical properties, source contributions, and radiative effects of BrC in Qinghai-
 596 Tibet Plateau, the observations equipped with the AE33 and the SP-AMS were carried out in July 2022
 597 in the Tibet background site (Yangbajing). For comparison, a simultaneous field observation was also
 598 conducted at the same periods in Guangzhou, a megacity with significant anthropogenic emissions. Our
 599 results reveal that the light absorption coefficient at 370 nm from total aerosols (Abs_{total} , $1.6 \pm 1.6 \text{ M m}^{-1}$)
 600 and BrC (Abs_{BrC} , $0.2 \pm 0.3 \text{ M m}^{-1}$) in Tibet were approximately an order of magnitude lower than those
 601 in Guangzhou (Abs_{total} , $13.2 \pm 7 \text{ M m}^{-1}$; Abs_{BrC} , $2.9 \pm 2 \text{ M m}^{-1}$), consistent with the extremely low mass
 602 concentrations of total aerosols and organic aerosols (OA) observed at the Tibetan site. The minimal
 603 aerosol loading and weak light absorption in Tibet underscore its pristine atmospheric background.

604 Despite a large discrepancy in absolute light absorption coefficient, the BrC light absorption
 605 contribution to total aerosols (15 % and 21 %) is comparable between the two sites at 370 nm,
 606 highlighting BrC's significant contribution to total aerosol light absorption in Tibet. The summarized
 607 field studies demonstrate a positive correlation between BrC fraction in Abs_{total} as a function of POA/OA

608 (R = 0.54), suggesting primary emissions contribute more effectively to BrC light absorption than BC,
609 and POA is a more important source of BrC light absorption than SOA at these two sites. Source
610 apportionment via the PMF–MLR method identified biomass–burning OA (BBOA) and hydrocarbon–
611 like OA (HOA) from vehicles as the major contributors (> 80 %) to the BrC light absorption in both sites.
612 The summarized field studies show that POA can account for 30–95 % of the BrC light absorption on a
613 global scale. All these finding signifies the critical role of primary emission in OA light absorption. The
614 main primary source for BrC includes biomass burning/biofuels, coal combustion, and vehicle emissions.

615 Diurnal variations of BrC and its sources exhibited distinct patterns with morning and nighttime
616 peaks. Weisang activity and traffic rush hours in Tibet significantly influenced BrC levels, underscoring
617 even remote regions' vulnerability to anthropogenic activities. Notably, traffic–related BrC contributions
618 remain substantial in Guangzhou and even in the Tibet background, which necessitates that explicit light
619 absorption parameters for fossil-derived BrC (e.g., from vehicle emissions) be considered in model
620 simulations. Current literature remains inconclusive regarding MAC differences between HOA and
621 BBOA, though fuel type, combustion efficiency, and aging effects critically influence BrC MAC,
622 emphasizing the need for enhanced field measurements and parameterization of source-specific MACs.

623 Based on this field study, the integrated total SFE of BrC across the 370–660 nm wavelength range
624 can account for approximately 7 % and 12 % of the BC (294.7 W g⁻¹ in Tibet and 286.3 W g⁻¹ in
625 Guangzhou). In total, primary emission contributes over 98 % of the total SFE at both sites. These
626 findings reinforce the urgency of controlling primary emissions and call for regional–specific
627 parameterizations in climate models to improve assessments of BrC's radiative effects. In general, our
628 study promotes the understanding of BrC dynamic variation and its sources at clean background Tibet
629 and typical urban areas, emphasizing the strong influences of anthropogenic to radiative forcing.

630

631 **Data availability**

632 The data shown in the paper are available on request from the corresponding authors
633 (weiwei@gig.ac.cn and shanhuang_eci@jnu.edu.cn).

634 **Author contributions**

635 WH, SH, PY, NM, BY, MS designed the research. SH, PY, NM, BY, WZ, ZL, LL, TP, TF, JW conducted
636 the field measurements. GZ and XB supported the AE33 instrument. WZ, LL, ZL, and YC analyzed the
637 data. LL and SH supported the SP-AMS data analysis and OA source analysis for the Tibet campaign.
638 WZ wrote the paper. WH, SH, ZL, TP, TF, JW, YC, GZ, XB, and XW reviewed and commented on the
639 paper.

640 **Competing interests.**

641 The authors declare that they have no conflict of interest.

642 **Acknowledgments**

643 This work has been supported by National Natural Science Foundation of China (Grant No 42375105),
644 the second Tibetan Plateau Scientific Expedition and Research Program (Grant No. 2019QZKK0604),
645 International Partnership Program of Chinese Academy of Sciences (Grant No.164GJHZ2023068FN),
646 Guangdong Foundation for Program of Science and Technology Research (Grant No 2023B1212060049),
647 Science Fund for Creative Research Groups of the National Natural Science Foundation of China (Grant
648 No 42321003). We appreciate Xiaomin Chen from Jinan University for providing assistance regarding
649 PMF analysis.
650

651 **References**

652 Andreae, M. O. and Gelencsér, A.: Black carbon or brown carbon? The nature of light-absorbing
653 carbonaceous aerosols, *Atmos. Chem. Phys.*, 6, 3131-3148, 10.5194/acp-6-3131-2006, 2006.

654 Bao, M., Zhang, Y.-L., Cao, F., Lin, Y.-C., Hong, Y., Fan, M., Zhang, Y., Yang, X., and Xie, F.: Light
655 absorption and source apportionment of water soluble humic-like substances (HULIS) in PM2.5 at
656 Nanjing, China, *Environmental Research*, 206, 10.1016/j.envres.2021.112554, 2022.

657 Barrett, T. E. and Sheesley, R. J.: Year-round optical properties and source characterization of Arctic
658 organic carbon aerosols on the North Slope Alaska, *Journal of Geophysical Research: Atmospheres*,
659 122, 9319-9331, 10.1002/2016jd026194, 2017.

660 Bond, T. C. and Bergstrom, R. W.: Light Absorption by Carbonaceous Particles: An Investigative Review,
661 *Aerosol Science and Technology*, 40, 27-67, 10.1080/02786820500421521, 2006.

662 Bond, T. C., Bergstrom, R. W. J. A. S., and Technology: Light Absorption by Carbonaceous Particles: An
663 Investigative Review, 40, 27 - 67, 2006.

664 Brown, H., Liu, X., Feng, Y., Jiang, Y., Wu, M., Lu, Z., Wu, C., Murphy, S., and Pokhrel, R.: Radiative
665 effect and climate impacts of brown carbon with the Community Atmosphere Model (CAM5),
666 *Atmospheric Chemistry and Physics*, 18, 17745-17768, 10.5194/acp-18-17745-2018, 2018.

667 Budisulistiorini, S. H., Riva, M., Williams, M., Chen, J., Itoh, M., Surratt, J. D., and Kuwata, M.: Light-
668 Absorbing Brown Carbon Aerosol Constituents from Combustion of Indonesian Peat and Biomass,
669 *Environ Sci Technol*, 51, 4415-4423, 10.1021/acs.est.7b00397, 2017.

670 Cai, Y., Ye, C., Chen, W., Hu, W., Song, W., Peng, Y., Huang, S., Qi, J., Wang, S., Wang, C., Wu, C.,
671 Wang, Z., Wang, B., Huang, X., He, L., Gligorovski, S., Yuan, B., Shao, M., and Wang, X.: The
672 important contribution of secondary formation and biomass burning to oxidized organic nitrogen
673 (OON) in a polluted urban area: insights from in situ measurements of a chemical ionization mass
674 spectrometer (CIMS), *Atmospheric Chemistry and Physics*, 23, 8855-8877, 10.5194/acp-23-8855-
675 2023, 2023.

676 Canonaco, F., Crippa, M., Slowik, J. G., Baltensperger, U., and Prévôt, A. S. H.: SoFi, an IGOR-based
677 interface for the efficient use of the generalized multilinear engine (ME-2) for the source
678 apportionment: ME-2 application to aerosol mass spectrometer data, *Atmospheric Measurement
679 Techniques*, 6, 3649-3661, 10.5194/amt-6-3649-2013, 2013.

680 Cappa, C. D., Zhang, X., Russell, L. M., Collier, S., Lee, A. K. Y., Chen, C. L., Betha, R., Chen, S., Liu,

681 J., Price, D. J., Sanchez, K. J., McMeeking, G. R., Williams, L. R., Onasch, T. B., Worsnop, D. R.,
682 Abbatt, J., and Zhang, Q.: Light Absorption by Ambient Black and Brown Carbon and its
683 Dependence on Black Carbon Coating State for Two California, USA, Cities in Winter and Summer,
684 *Journal of Geophysical Research: Atmospheres*, 124, 1550-1577, 10.1029/2018jd029501, 2019.

685 Cappa, C. D., Onasch, T. B., Massoli, P., Worsnop, D. R., Bates, T. S., Cross, E. S., Davidovits, P., Hakala,
686 J., Hayden, K. L., Jobson, B. T., Kolesar, K. R., Lack, D. A., Lerner, B. M., Li, S.-M., Mellon, D.,
687 Nuaaman, I., Olfert, J. S., Petäjä, T., Quinn, P. K., Song, C., Subramanian, R., Williams, E. J., and
688 Zaveri, R. A.: Radiative Absorption Enhancements Due to the Mixing State of Atmospheric Black
689 Carbon, 337, 1078-1081, doi:10.1126/science.1223447, 2012.

690 Chelluboyina, G. S., Kapoor, T. S., and Chakrabarty, R. K.: Dark brown carbon from wildfires: a potent
691 snow radiative forcing agent?, *npj Climate and Atmospheric Science*, 7, 10.1038/s41612-024-
692 00738-7, 2024.

693 Chen, P., Kang, S., Hu, Y., Pu, T., Liu, Y., Wang, S., Rai, M., Wang, K., Tripathee, L., and Li, C.: South
694 and Southeast Asia controls black carbon characteristics of Meili Snow Mountains in southeast
695 Tibetan Plateau, *Science of The Total Environment*, 927, 10.1016/j.scitotenv.2024.172262, 2024.

696 Chen, W., Ye, Y., Hu, W., Zhou, H., Pan, T., Wang, Y., Song, W., Song, Q., Ye, C., Wang, C., Wang, B.,
697 Huang, S., Yuan, B., Zhu, M., Lian, X., Zhang, G., Bi, X., Jiang, F., Liu, J., Canonaco, F., Prevot,
698 A. S. H., Shao, M., and Wang, X.: Real-Time Characterization of Aerosol Compositions, Sources,
699 and Aging Processes in Guangzhou During PRIDE-GBA 2018 Campaign, *Journal of Geophysical
700 Research: Atmospheres*, 126, 10.1029/2021jd035114, 2021.

701 Chen, Y. and Bond, T. C.: Light absorption by organic carbon from wood combustion, *Atmos. Chem.
702 Phys.*, 10, 1773-1787, 10.5194/acp-10-1773-2010, 2010.

703 Chen, Y., Xie, X., Shi, Z., Li, Y., Gai, X., Wang, J., Li, H., Wu, Y., Zhao, X., Chen, M., and Ge, X.: Brown
704 carbon in atmospheric fine particles in Yangzhou, China: Light absorption properties and source
705 apportionment, *Atmospheric Research*, 244, 10.1016/j.atmosres.2020.105028, 2020.

706 Cheng, Y., He, K. B., Zheng, M., Duan, F. K., Du, Z. Y., Ma, Y. L., Tan, J. H., Yang, F. M., Liu, J. M.,
707 Zhang, X. L., Weber, R. J., Bergin, M. H., and Russell, A. G.: Mass absorption efficiency of
708 elemental carbon and water-soluble organic carbon in Beijing, China, *Atmos. Chem. Phys.*, 11,
709 11497-11510, 10.5194/acp-11-11497-2011, 2011.

710 Chung, C. E., Ramanathan, V., and Decremer, D.: Observationally constrained estimates of carbonaceous
711 aerosol radiative forcing, Proc Natl Acad Sci U S A, 109, 11624-11629, 10.1073/pnas.1203707109,
712 2012.

713 Chylek, P. and Wong, J.: Effect of absorbing aerosols on global radiation budget, Geophysical Research
714 Letters, 22, 929-931, <https://doi.org/10.1029/95GL00800>, 1995.

715 Collaud Coen, M., Weingartner, E., Apituley, A., Ceburnis, D., Fierz-Schmidhauser, R., Flentje, H.,
716 Henzing, J. S., Jennings, S. G., Moerman, M., Petzold, A., Schmid, O., and Baltensperger, U.:
717 Minimizing light absorption measurement artifacts of the Aethalometer: evaluation of five
718 correction algorithms, Atmos. Meas. Tech., 3, 457-474, 10.5194/amt-3-457-2010, 2010.

719 Corr, C. A., Hall, S. R., Ullmann, K., Anderson, B. E., Beyersdorf, A. J., Thornhill, K. L., Cubison, M.
720 J., Jimenez, J. L., Wisthaler, A., and Dibb, J. E.: Spectral absorption of biomass burning aerosol
721 determined from retrieved single scattering albedo during ARCTAS, Atmos. Chem. Phys., 12,
722 10505-10518, 10.5194/acp-12-10505-2012, 2012.

723 de Sá, S. S., Rizzo, L. V., Palm, B. B., Campuzano-Jost, P., Day, D. A., Yee, L. D., Wernis, R., Isaacman-
724 VanWertz, G., Brito, J., Carbone, S., Liu, Y. J., Sedlacek, A., Springston, S., Goldstein, A. H.,
725 Barbosa, H. M. J., Alexander, M. L., Artaxo, P., Jimenez, J. L., and Martin, S. T.: Contributions of
726 biomass-burning, urban, and biogenic emissions to the concentrations and light-absorbing
727 properties of particulate matter in central Amazonia during the dry season, Atmos. Chem. Phys., 19,
728 7973-8001, 10.5194/acp-19-7973-2019, 2019.

729 Drinovec, L., Močnik, G., Zotter, P., Prévôt, A. S. H., Ruckstuhl, C., Coz, E., Rupakheti, M., Sciare, J.,
730 Müller, T., Wiedensohler, A., and Hansen, A. D. A.: The "dual-spot" Aethalometer: an improved
731 measurement of aerosol black carbon with real-time loading compensation, Atmos. Meas. Tech., 8,
732 1965-1979, 10.5194/amt-8-1965-2015, 2015.

733 Du, Z., He, K., Cheng, Y., Duan, F., Ma, Y., Liu, J., Zhang, X., Zheng, M., and Weber, R.: A yearlong
734 study of water-soluble organic carbon in Beijing II: Light absorption properties, Atmospheric
735 Environment, 89, 235-241, 10.1016/j.atmosenv.2014.02.022, 2014.

736 Efremenko, D. and Kokhanovsky, A.: Radiative Transfer Models, in: Foundations of Atmospheric
737 Remote Sensing, edited by: Efremenko, D., and Kokhanovsky, A., Springer International Publishing,
738 Cham, 149-232, 10.1007/978-3-030-66745-0_4, 2021.

739 Feng, Y., Ramanathan, V., and Kotamarthi, V. R.: Brown carbon: a significant atmospheric absorber of
740 solar radiation?, *Atmos. Chem. Phys.*, 13, 8607-8621, 10.5194/acp-13-8607-2013, 2013.

741 Fröhlich, R., Cubison, M. J., Slowik, J. G., Bukowiecki, N., Prévôt, A. S. H., Baltensperger, U., Schneider,
742 J., Kimmel, J. R., Gonin, M., Rohner, U., Worsnop, D. R., and Jayne, J. T.: The ToF-ACSM: a
743 portable aerosol chemical speciation monitor with TOFMS detection, *Atmospheric Measurement
Techniques*, 6, 3225-3241, 10.5194/amt-6-3225-2013, 2013.

744 Gustafsson, O. and Ramanathan, V.: Convergence on climate warming by black carbon aerosols, *Proc
746 Natl Acad Sci U S A*, 113, 4243-4245, 10.1073/pnas.1603570113, 2016.

747 Hems, R. F. and Abbatt, J. P. D.: Aqueous Phase Photo-oxidation of Brown Carbon Nitrophenols:
748 Reaction Kinetics, Mechanism, and Evolution of Light Absorption, *ACS Earth and Space Chemistry*,
749 2, 225-234, 10.1021/acsearthspacechem.7b00123, 2018.

750 Hems, R. F., Schnitzler, E. G., Liu-Kang, C., Cappa, C. D., and Abbatt, J. P. D.: Aging of Atmospheric
751 Brown Carbon Aerosol, *ACS Earth and Space Chemistry*, 5, 722-748,
752 10.1021/acsearthspacechem.0c00346, 2021.

753 Hu, W., Hu, M., Hu, W., Jimenez, J. L., Yuan, B., Chen, W., Wang, M., Wu, Y., Chen, C., Wang, Z., Peng,
754 J., Zeng, L., and Shao, M.: Chemical composition, sources, and aging process of submicron aerosols
755 in Beijing: Contrast between summer and winter, *Journal of Geophysical Research: Atmospheres*,
756 121, 1955-1977, 10.1002/2015jd024020, 2016.

757 Hu, W. W., Hu, M., Yuan, B., Jimenez, J. L., Tang, Q., Peng, J. F., Hu, W., Shao, M., Wang, M., Zeng, L.
758 M., Wu, Y. S., Gong, Z. H., Huang, X. F., and He, L. Y.: Insights on organic aerosol aging and the
759 influence of coal combustion at a regional receptor site of central eastern China, *Atmospheric
760 Chemistry and Physics*, 13, 10095-10112, 10.5194/acp-13-10095-2013, 2013.

761 Huang, R.-J., Yuan, W., Yang, L., Yang, H., Cao, W., Guo, J., Zhang, N., Zhu, C., Wu, Y., and Zhang, R.:
762 Concentration, optical characteristics, and emission factors of brown carbon emitted by on-road
763 vehicles, *Science of The Total Environment*, 810, 10.1016/j.scitotenv.2021.151307, 2022.

764 Jacobson, M. Z.: Strong radiative heating due to the mixing state of black carbon in atmospheric aerosols,
765 *Nature*, 409, 695-697, 10.1038/35055518, 2001.

766 Jiang, H., Frie, A. L., Lavi, A., Chen, J. Y., Zhang, H., Bahreini, R., and Lin, Y.-H.: Brown Carbon
767 Formation from Nighttime Chemistry of Unsaturated Heterocyclic Volatile Organic Compounds,

768 Environmental Science & Technology Letters, 6, 184-190, 10.1021/acs.estlett.9b00017, 2019.

769 Kang, S., Zhang, Q., Qian, Y., Ji, Z., Li, C., Cong, Z., Zhang, Y., Guo, J., Du, W., Huang, J., You, Q.,
770 Panday, A. K., Rupakheti, M., Chen, D., Gustafsson, O., Thiemen, M. H., and Qin, D.: Linking
771 atmospheric pollution to cryospheric change in the Third Pole region: current progress and future
772 prospects, Natl Sci Rev, 6, 796-809, 10.1093/nsr/nwz031, 2019.

773 Kaskaoutis, D. G., Grivas, G., Stavroulas, I., Bougiatioti, A., Liakakou, E., Dumka, U. C., Gerasopoulos,
774 E., and Mihalopoulos, N.: Apportionment of black and brown carbon spectral absorption sources in
775 the urban environment of Athens, Greece, during winter, Science of The Total Environment, 801,
776 10.1016/j.scitotenv.2021.149739, 2021.

777 Kasthuriarachchi, N. Y., Rivellini, L. H., Adam, M. G., and Lee, A. K. Y.: Light Absorbing Properties of
778 Primary and Secondary Brown Carbon in a Tropical Urban Environment, Environ Sci Technol, 54,
779 10808-10819, 10.1021/acs.est.0c02414, 2020a.

780 Kasthuriarachchi, N. Y., Rivellini, L. H., Chen, X., Li, Y. J., and Lee, A. K. Y.: Effect of Relative Humidity
781 on Secondary Brown Carbon Formation in Aqueous Droplets, Environ Sci Technol, 54, 13207-
782 13216, 10.1021/acs.est.0c01239, 2020b.

783 Kirchstetter, T. W. and Thatcher, T. L.: Contribution of organic carbon to wood smoke particulate matter
784 absorption of solar radiation, Atmos. Chem. Phys., 12, 6067-6072, 10.5194/acp-12-6067-2012,
785 2012.

786 Kirchstetter, T. W., Novakov, T., and Hobbs, P. V.: Evidence that the spectral dependence of light
787 absorption by aerosols is affected by organic carbon, Journal of Geophysical Research: Atmospheres,
788 109, n/a-n/a, 10.1029/2004jd004999, 2004.

789 Lack, D. A. and Langridge, J. M.: On the attribution of black and brown carbon light absorption using
790 the Ångström exponent, Atmos. Chem. Phys., 13, 10535-10543, 10.5194/acp-13-10535-2013, 2013.

791 Lack, D. A., Moosmuller, H., McMeeking, G. R., Chakrabarty, R. K., and Baumgardner, D.:
792 Characterizing elemental, equivalent black, and refractory black carbon aerosol particles: a review
793 of techniques, their limitations and uncertainties, Anal Bioanal Chem, 406, 99-122,
794 10.1007/s00216-013-7402-3, 2014.

795 Lack, D. A., Richardson, M. S., Law, D., Langridge, J. M., Cappa, C. D., McLaughlin, R. J., and Murphy,
796 D. M.: Aircraft Instrument for Comprehensive Characterization of Aerosol Optical Properties, Part

797 2: Black and Brown Carbon Absorption and Absorption Enhancement Measured with Photo
798 Acoustic Spectroscopy, Aerosol Science and Technology, 46, 555-568,
799 10.1080/02786826.2011.645955, 2012.

800 Lambe, A. T., Cappa, C. D., Massoli, P., Onasch, T. B., Forestieri, S. D., Martin, A. T., Cummings, M. J.,
801 Croasdale, D. R., Brune, W. H., Worsnop, D. R., and Davidovits, P.: Relationship between oxidation
802 level and optical properties of secondary organic aerosol, Environ Sci Technol, 47, 6349-6357,
803 10.1021/es401043j, 2013.

804 Laskin, A., Laskin, J., and Nizkorodov, S. A.: Chemistry of atmospheric brown carbon, Chem Rev, 115,
805 4335-4382, 10.1021/cr5006167, 2015.

806 Laskin, J., Laskin, A., Nizkorodov, S. A., Roach, P., Eckert, P., Gilles, M. K., Wang, B., Lee, H. J., and
807 Hu, Q.: Molecular selectivity of brown carbon chromophores, Environ Sci Technol, 48, 12047-
808 12055, 10.1021/es503432r, 2014.

809 Lee, H. J., Aiona, P. K., Laskin, A., Laskin, J., and Nizkorodov, S. A.: Effect of Solar Radiation on the
810 Optical Properties and Molecular Composition of Laboratory Proxies of Atmospheric Brown
811 Carbon, Environmental Science & Technology, 48, 10217-10226, 10.1021/es502515r, 2014.

812 Lei, Y., Shen, Z., Zhang, T., Lu, D., Zeng, Y., Zhang, Q., Xu, H., Bei, N., Wang, X., and Cao, J.: High
813 time resolution observation of PM2.5 Brown carbon over Xi'an in northwestern China: Seasonal
814 variation and source apportionment, Chemosphere, 237, 10.1016/j.chemosphere.2019.124530,
815 2019.

816 Li, C., He, Q., Hettiyadura, A. P. S., Kafer, U., Shmul, G., Meidan, D., Zimmermann, R., Brown, S. S.,
817 George, C., Laskin, A., and Rudich, Y.: Formation of Secondary Brown Carbon in Biomass Burning
818 Aerosol Proxies through NO(3) Radical Reactions, Environ Sci Technol, 54, 1395-1405,
819 10.1021/acs.est.9b05641, 2020.

820 Li, X., Kang, S., He, X., Qu, B., Tripathee, L., Jing, Z., Paudyal, R., Li, Y., Zhang, Y., Yan, F., Li, G., and
821 Li, C.: Light-absorbing impurities accelerate glacier melt in the Central Tibetan Plateau, Sci Total
822 Environ, 587-588, 482-490, 10.1016/j.scitotenv.2017.02.169, 2017.

823 Li, Y., Fu, T.-M., Yu, J. Z., Zhang, A., Yu, X., Ye, J., Zhu, L., Shen, H., Wang, C., Yang, X., Tao, S., Chen,
824 Q., Li, Y., Li, L., Che, H., and Heald, C. L.: Nitrogen dominates global atmospheric organic aerosol
825 absorption, 387, 989-995, doi:10.1126/science.adr4473, 2025.

826 Liu, D., Whitehead, J., Alfarra, M. R., Reyes-Villegas, E., Spracklen, Dominick V., Reddington, Carly L.,
827 Kong, S., Williams, Paul I., Ting, Y.-C., Haslett, S., Taylor, Jonathan W., Flynn, Michael J., Morgan,
828 William T., McFigans, G., Coe, H., and Allan, James D.: Black-carbon absorption enhancement in
829 the atmosphere determined by particle mixing state, *Nature Geoscience*, 10, 184-188,
830 10.1038/ngeo2901, 2017.

831 Liu, Y., Wang, Y., Cao, Y., Yang, X., Zhang, T., Luan, M., Lyu, D., Hansen, A. D. A., Liu, B., and Zheng,
832 M.: Impacts of COVID-19 on Black Carbon in Two Representative Regions in China: Insights
833 Based on Online Measurement in Beijing and Tibet, *Geophys Res Lett*, 48, e2021GL092770,
834 10.1029/2021GL092770, 2021.

835 Luo, B., Kuang, Y., Huang, S., Song, Q., Hu, W., Li, W., Peng, Y., Chen, D., Yue, D., Yuan, B., and Shao,
836 M.: Parameterizations of size distribution and refractive index of biomass burning organic aerosol
837 with black carbon content, *Atmos. Chem. Phys.*, 22, 12401-12415, 10.5194/acp-22-12401-2022,
838 2022.

839 Martinsson, J., Eriksson, A. C., Nielsen, I. E., Malmborg, V. B., Ahlberg, E., Andersen, C., Lindgren, R.,
840 Nystrom, R., Nordin, E. Z., Brune, W. H., Svenningsson, B., Swietlicki, E., Boman, C., and Pagels,
841 J. H.: Impacts of Combustion Conditions and Photochemical Processing on the Light Absorption of
842 Biomass Combustion Aerosol, *Environ Sci Technol*, 49, 14663-14671, 10.1021/acs.est.5b03205,
843 2015.

844 Middlebrook, A. M., Bahreini, R., Jimenez, J. L., and Canagaratna, M. R.: Evaluation of Composition-
845 Dependent Collection Efficiencies for the Aerodyne Aerosol Mass Spectrometer using Field Data,
846 *Aerosol Science and Technology*, 46, 258-271, 10.1080/02786826.2011.620041, 2012.

847 Ming, J., Xiao, C., Du, Z., and Yang, X.: An overview of black carbon deposition in High Asia glaciers
848 and its impacts on radiation balance, *Advances in Water Resources*, 55, 80-87,
849 10.1016/j.advwatres.2012.05.015, 2013.

850 Mo, Y., Li, J., Liu, J., Zhong, G., Cheng, Z., Tian, C., Chen, Y., and Zhang, G.: The influence of solvent
851 and pH on determination of the light absorption properties of water-soluble brown carbon,
852 *Atmospheric Environment*, 161, 90-98, 10.1016/j.atmosenv.2017.04.037, 2017.

853 Moschos, V., Christensen, C., Mouton, M., Fiddler, M. N., Isolabella, T., Mazzei, F., Massabò, D., Turpin,
854 B. J., Bililign, S., and Surratt, J. D.: Quantifying the Light-Absorption Properties and Molecular

855 Composition of Brown Carbon Aerosol from Sub-Saharan African Biomass Combustion,
856 Environmental Science & Technology, 10.1021/acs.est.3c09378, 2024.

857 Ni, H., Huang, R. J., Pieber, S. M., Corbin, J. C., Stefenelli, G., Pospisilova, V., Klein, F., Gysel-Beer,
858 M., Yang, L., Baltensperger, U., Haddad, I. E., Slowik, J. G., Cao, J., Prevot, A. S. H., and Dusek,
859 U.: Brown Carbon in Primary and Aged Coal Combustion Emission, Environ Sci Technol, 55, 5701-
860 5710, 10.1021/acs.est.0c08084, 2021.

861 Onasch, T. B., Trimborn, A., Fortner, E. C., Jayne, J. T., Kok, G. L., Williams, L. R., Davidovits, P., and
862 Worsnop, D. R.: Soot Particle Aerosol Mass Spectrometer: Development, Validation, and Initial
863 Application, Aerosol Science and Technology, 46, 804-817, 10.1080/02786826.2012.663948, 2012.

864 Peng, J., Hu, M., Guo, S., Du, Z., Zheng, J., Shang, D., Levy Zamora, M., Zeng, L., Shao, M., Wu, Y. S.,
865 Zheng, J., Wang, Y., Glen, C. R., Collins, D. R., Molina, M. J., and Zhang, R.: Markedly enhanced
866 absorption and direct radiative forcing of black carbon under polluted urban environments, Proc
867 Natl Acad Sci U S A, 113, 4266-4271, 10.1073/pnas.1602310113, 2016.

868 Phillips, S. M., Bellcross, A. D., and Smith, G. D.: Light Absorption by Brown Carbon in the
869 Southeastern United States is pH-dependent, Environ Sci Technol, 51, 6782-6790,
870 10.1021/acs.est.7b01116, 2017.

871 Powelson, M. H., Espelien, B. M., Hawkins, L. N., Galloway, M. M., and De Haan, D. O.: Brown carbon
872 formation by aqueous-phase carbonyl compound reactions with amines and ammonium sulfate,
873 Environ Sci Technol, 48, 985-993, 10.1021/es4038325, 2014.

874 Qin, Y. M., Tan, H. B., Li, Y. J., Li, Z. J., Schurman, M. I., Liu, L., Wu, C., and Chan, C. K.: Chemical
875 characteristics of brown carbon in atmospheric particles at a suburban site near Guangzhou, China,
876 Atmospheric Chemistry and Physics, 18, 16409-16418, 10.5194/acp-18-16409-2018, 2018.

877 Retama, A., Ramos-Cerón, M., Rivera-Hernández, O., Allen, G., and Velasco, E.: Aerosol optical
878 properties and brown carbon in Mexico City, Environmental Science: Atmospheres, 2, 315-334,
879 10.1039/d2ea00006g, 2022.

880 Saleh, R.: From Measurements to Models: Toward Accurate Representation of Brown Carbon in Climate
881 Calculations, Current Pollution Reports, 6, 90-104, 10.1007/s40726-020-00139-3, 2020.

882 Saleh, R., Robinson, E. S., Tkacik, D. S., Ahern, A. T., Liu, S., Aiken, A. C., Sullivan, R. C., Presto, A.
883 A., Dubey, M. K., Yokelson, R. J., Donahue, N. M., and Robinson, A. L.: Brownness of organics in

884 aerosols from biomass burning linked to their black carbon content, *Nature Geoscience*, 7, 647-650,
885 10.1038/ngeo2220, 2014.

886 Shen, G., Xiong, R., Cheng, H., and Tao, S.: Rural residential energy carrier structure and primary
887 PM_{2.5} emissions from the Qinghai-Tibet Plateau, *Chinese Science
888 Bulletin*, 66, 1900-1911, 10.1360/tb-2020-0408, 2021.

889 Singh, A., Rastogi, N., Kumar, V., Slowik, J. G., Satish, R., Lalchandani, V., Thamban, N. M., Rai, P.,
890 Bhattu, D., Vats, P., Ganguly, D., Tripathi, S. N., and Prévôt, A. S. H.: Sources and characteristics
891 of light-absorbing fine particulates over Delhi through the synergy of real-time optical and chemical
892 measurements, *ATMOSPHERIC ENVIRONMENT*, 252, 10.1016/j.atmosenv.2021.118338, 2021.

893 Sumlin, B. J., Pandey, A., Walker, M. J., Pattison, R. S., Williams, B. J., and Chakrabarty, R. K.:
894 Atmospheric Photooxidation Diminishes Light Absorption by Primary Brown Carbon Aerosol from
895 Biomass Burning, *Environmental Science & Technology Letters*, 4, 540-545,
896 10.1021/acs.estlett.7b00393, 2017.

897 Sun, J., Xie, C., Xu, W., Chen, C., Ma, N., Xu, W., Lei, L., Li, Z., He, Y., Qiu, Y., Wang, Q., Pan, X., Su,
898 H., Cheng, Y., Wu, C., Fu, P., Wang, Z., and Sun, Y.: Light absorption of black carbon and brown
899 carbon in winter in North China Plain: comparisons between urban and rural sites, *Science of The
900 Total Environment*, 770, 10.1016/j.scitotenv.2020.144821, 2021.

901 Tang, J., Li, J., Su, T., Han, Y., Mo, Y., Jiang, H., Cui, M., Jiang, B., Chen, Y., Tang, J., Song, J., Peng, P.
902 a., and Zhang, G.: Molecular compositions and optical properties of dissolved brown carbon in
903 biomass burning, coal combustion, and vehicle emission aerosols illuminated by excitation–
904 emission matrix spectroscopy and Fourier transform ion cyclotron resonance mass spectrometry
905 analysis, *Atmospheric Chemistry and Physics*, 20, 2513-2532, 10.5194/acp-20-2513-2020, 2020.

906 Tang, S., Li, F., Lv, J., Liu, L., Wu, G., Wang, Y., Yu, W., Wang, Y., and Jiang, G.: Unexpected molecular
907 diversity of brown carbon formed by Maillard-like reactions in aqueous aerosols, *Chem Sci*, 13,
908 8401-8411, 10.1039/d2sc02857c, 2022.

909 Tian, J., Wang, Q., Ma, Y., Wang, J., Han, Y., and Cao, J.: Impacts of biomass burning and photochemical
910 processing on the light absorption of brown carbon in the southeastern Tibetan Plateau, *Atmospheric
911 Chemistry and Physics*, 23, 1879-1892, 10.5194/acp-23-1879-2023, 2023.

912 Ulbrich, I. M., Canagaratna, M. R., Zhang, Q., Worsnop, D. R., and Jimenez, J. L.: Interpretation of

913 organic components from Positive Matrix Factorization of aerosol mass spectrometric data,
914 Atmospheric Chemistry and Physics, 9, 2891-2918, 10.5194/acp-9-2891-2009, 2009.

915 Usha, K. H., Nair, V. S., and Babu, S. S.: Effects of Aerosol-Induced Snow Albedo Feedback on the
916 Seasonal Snowmelt Over the Himalayan Region, Water Resources Research, 58,
917 10.1029/2021wr030140, 2022.

918 Wang, D., Shen, Z., Zhang, Q., Lei, Y., Zhang, T., Huang, S., Sun, J., Xu, H., and Cao, J.: Winter brown
919 carbon over six of China's megacities: light absorption, molecular characterization, and improved
920 source apportionment revealed by multilayer perceptron neural network, Atmospheric Chemistry
921 and Physics, 22, 14893-14904, 10.5194/acp-22-14893-2022, 2022a.

922 Wang, L. Y., Qu, Y., Wang, N., Shi, J. L., Zhou, Y., Cao, Y., Yang, X. L., Shi, Y. Q., Liu, S. X., Zhu, C.
923 S., and Cao, J. J.: Long-term spatial distribution and implication of black and brown carbon in the
924 Tibetan Plateau, Sci Total Environ, 945, 174093, 10.1016/j.scitotenv.2024.174093, 2024.

925 Wang, Q., Zhou, Y., Ma, N., Zhu, Y., Zhao, X., Zhu, S., Tao, J., Hong, J., Wu, W., Cheng, Y., and Su, H.:
926 Review of Brown Carbon Aerosols in China: Pollution Level, Optical Properties, and Emissions,
927 Journal of Geophysical Research: Atmospheres, 127, 10.1029/2021jd035473, 2022b.

928 Wang, Q., Han, Y., Ye, J., Liu, S., Pongpiachan, S., Zhang, N., Han, Y., Tian, J., Wu, C., Long, X., Zhang,
929 Q., Zhang, W., Zhao, Z., and Cao, J.: High Contribution of Secondary Brown Carbon to Aerosol
930 Light Absorption in the Southeastern Margin of Tibetan Plateau, Geophysical Research Letters, 46,
931 4962-4970, 10.1029/2019gl082731, 2019a.

932 Wang, Q., Ye, J., Wang, Y., Zhang, T., Ran, W., Wu, Y., Tian, J., Li, L., Zhou, Y., Hang Ho, S. S., Dang,
933 B., Zhang, Q., Zhang, R., Chen, Y., Zhu, C., and Cao, J.: Wintertime Optical Properties of Primary
934 and Secondary Brown Carbon at a Regional Site in the North China Plain, Environmental Science
935 & Technology, 53, 12389-12397, 10.1021/acs.est.9b03406, 2019b.

936 Wang, X., Heald, C. L., Liu, J., Weber, R. J., Campuzano-Jost, P., Jimenez, J. L., Schwarz, J. P., and
937 Perring, A. E.: Exploring the observational constraints on the simulation of brown carbon,
938 Atmospheric Chemistry and Physics, 18, 635-653, 10.5194/acp-18-635-2018, 2018.

939 Wang, X., Chakrabarty, R. K., Schwarz, J. P., Murphy, S. M., Levin, E. J. T., Howell, S. G., Guo, H.,
940 Campuzano-Jost, P., and Jimenez, J. L.: Dark brown carbon from biomass burning contributes to
941 significant global-scale positive forcing, One Earth, 10.1016/j.oneear.2025.101205, 2025.

942 Wang, Y., Hu, M., Lin, P., Guo, Q., Wu, Z., Li, M., Zeng, L., Song, Y., Zeng, L., Wu, Y., Guo, S., Huang,
943 X., and He, L.: Molecular Characterization of Nitrogen-Containing Organic Compounds in Humic-
944 like Substances Emitted from Straw Residue Burning, *Environmental Science & Technology*, 51,
945 5951-5961, 10.1021/acs.est.7b00248, 2017.

946 Wang, Y. Q.: An Open Source Software Suite for Multi-Dimensional Meteorological Data
947 Computation and Visualisation, *Journal of Open Research Software*, 7, 10.5334/jors.267, 2019.

948 Washenfelder, R. A., Attwood, A. R., Brock, C. A., Guo, H., Xu, L., Weber, R. J., Ng, N. L., Allen, H.
949 M., Ayres, B. R., Baumann, K., Cohen, R. C., Draper, D. C., Duffey, K. C., Edgerton, E., Fry, J. L.,
950 Hu, W. W., Jimenez, J. L., Palm, B. B., Romer, P., Stone, E. A., Wooldridge, P. J., and Brown, S. S.:
951 Biomass burning dominates brown carbon absorption in the rural southeastern United States,
952 *Geophysical Research Letters*, 42, 653-664, <https://doi.org/10.1002/2014GL062444>, 2015.

953 Wong, J. P. S., Nenes, A., and Weber, R. J.: Changes in Light Absorptivity of Molecular Weight Separated
954 Brown Carbon Due to Photolytic Aging, *Environ Sci Technol*, 51, 8414-8421,
955 10.1021/acs.est.7b01739, 2017.

956 Xiang, Y., Li, X., Zhang, T., Cheng, Q., Yan, C., Liu, X., Liu, Y., Wang, Y., Kang, S., Ding, X., and Zheng,
957 M.: Characteristics and Sources of Organic Aerosol in PM2.5 at Yangbajing in Tibetan Plateau,
958 *Atmospheric Environment*, 333, 10.1016/j.atmosenv.2024.120662, 2024.

959 Xie, M., Hays, M. D., and Holder, A. L.: Light-absorbing organic carbon from prescribed and laboratory
960 biomass burning and gasoline vehicle emissions, *Sci Rep*, 7, 7318, 10.1038/s41598-017-06981-8,
961 2017.

962 Xu, J., Zhang, Q., Shi, J., Ge, X., Xie, C., Wang, J., Kang, S., Zhang, R., and Wang, Y.: Chemical
963 characteristics of submicron particles at the central Tibetan Plateau: insights from aerosol mass
964 spectrometry, *Atmospheric Chemistry and Physics*, 18, 427-443, 10.5194/acp-18-427-2018, 2018.

965 Xu, L., Lin, G., Liu, X., Wu, C., Wu, Y., and Lou, S.: Constraining Light Absorption of Brown Carbon
966 in China and Implications for Aerosol Direct Radiative Effect, *Geophysical Research Letters*, 51,
967 10.1029/2024gl109861, 2024.

968 Yao, T., Thompson, L. G., Mosbrugger, V., Zhang, F., Ma, Y., Luo, T., Xu, B., Yang, X., Joswiak, D. R.,
969 Wang, W., Joswiak, M. E., Devkota, L. P., Tayal, S., Jilani, R., and Fayziev, R.: Third Pole
970 Environment (TPE), *Environmental Development*, 3, 52-64, 10.1016/j.envdev.2012.04.002, 2012.

971 Yu, L., Smith, J., Laskin, A., George, K. M., Anastasio, C., Laskin, J., Dillner, A. M., and Zhang, Q.:
972 Molecular transformations of phenolic SOA during photochemical aging in the aqueous phase:
973 competition among oligomerization, functionalization, and fragmentation, *Atmospheric Chemistry*
974 and *Physics*, 16, 4511-4527, 10.5194/acp-16-4511-2016, 2016.

975 Yue, S., Bikkina, S., Gao, M., Barrie, L. A., Kawamura, K., and Fu, P.: Sources and Radiative Absorption
976 of Water-Soluble Brown Carbon in the High Arctic Atmosphere, *Geophysical Research Letters*, 46,
977 14881-14891, 10.1029/2019gl085318, 2019.

978 Yue, S., Zhu, J., Chen, S., Xie, Q., Li, W., Li, L., Ren, H., Su, S., Li, P., Ma, H., Fan, Y., Cheng, B., Wu,
979 L., Deng, J., Hu, W., Ren, L., Wei, L., Zhao, W., Tian, Y., Pan, X., Sun, Y., Wang, Z., Wu, F., Liu,
980 C.-Q., Su, H., Penner, J. E., Pöschl, U., Andreae, M. O., Cheng, Y., and Fu, P.: Brown carbon from
981 biomass burning imposes strong circum-Arctic warming, *One Earth*, 5, 293-304,
982 10.1016/j.oneear.2022.02.006, 2022.

983 Zhai, J., Yang, X., Li, L., Bai, B., Liu, P., Huang, Y., Fu, T.-M., Zhu, L., Zeng, Z., Tao, S., Lu, X., Ye, X.,
984 Wang, X., Wang, L., and Chen, J.: Absorption Enhancement of Black Carbon Aerosols Constrained
985 by Mixing-State Heterogeneity, *Environmental Science & Technology*, 56, 1586-1593,
986 10.1021/acs.est.1c06180, 2022.

987 Zhang, Q., Jimenez, J. L., Canagaratna, M. R., Ulbrich, I. M., Ng, N. L., Worsnop, D. R., and Sun, Y.:
988 Understanding atmospheric organic aerosols via factor analysis of aerosol mass spectrometry: a
989 review, *Anal Bioanal Chem*, 401, 3045-3067, 10.1007/s00216-011-5355-y, 2011.

990 Zhang, Q., Shen, Z., Zhang, L., Zeng, Y., Ning, Z., Zhang, T., Lei, Y., Wang, Q., Li, G., Sun, J., Westerdahl,
991 D., Xu, H., and Cao, J.: Investigation of Primary and Secondary Particulate Brown Carbon in Two
992 Chinese Cities of Xi'an and Hong Kong in Wintertime, *Environmental Science & Technology*, 54,
993 3803-3813, 10.1021/acs.est.9b05332, 2020a.

994 Zhang, X., Xu, J., and Kang, S.: Chemical characterization of submicron particulate matter (PM1)
995 emitted by burning highland barley in the northeastern part of the Qinghai-Tibet Plateau,
996 *Atmospheric Environment*, 224, 10.1016/j.atmosenv.2020.117351, 2020b.

997 Zhang, X., Xu, J., Zhai, L., and Zhao, W.: Characterization of Aerosol Properties from the Burning
998 Emissions of Typical Residential Fuels on the Tibetan Plateau, *Environ Sci Technol*,
999 10.1021/acs.est.2c04211, 2022a.

1000 Zhang, X., Xu, J., Kang, S., Sun, J., Shi, J., Gong, C., Sun, X., Du, H., Ge, X., and Zhang, Q.: Regional
1001 Differences in the Light Absorption Properties of Fine Particulate Matter Over the Tibetan Plateau:
1002 Insights From HR-ToF-AMS and Aethalometer Measurements, *Journal of Geophysical Research: Atmospheres*, 126, 10.1029/2021jd035562, 2021.

1003
1004 Zhang, Y., Wang, Q., Tian, J., Li, Y., Liu, H., Ran, W., Han, Y., Prévôt, A. S. H., and Cao, J.: Impact of
1005 COVID-19 lockdown on the optical properties and radiative effects of urban brown carbon aerosol,
1006 *Geoscience Frontiers*, 13, 101320, <https://doi.org/10.1016/j.gsf.2021.101320>, 2022b.

1007 Zhang, Y., Albinet, A., Petit, J.-E., Jacob, V., Chevrier, F., Gille, G., Pontet, S., Chrétien, E., Dominik-
1008 Sègue, M., Levigoureux, G., Močnik, G., Gros, V., Jaffrezo, J.-L., and Favez, O.: Substantial brown
1009 carbon emissions from wintertime residential wood burning over France, *Science of The Total
1010 Environment*, 743, 10.1016/j.scitotenv.2020.140752, 2020c.

1011 Zhao, R., Lee, A. K. Y., Huang, L., Li, X., Yang, F., and Abbatt, J. P. D.: Photochemical processing of
1012 aqueous atmospheric brown carbon, *Atmospheric Chemistry and Physics*, 15, 6087-6100,
1013 10.5194/acp-15-6087-2015, 2015.

1014 Zhao, W., Zhang, X., Zhai, L., Shen, X., and Xu, J.: Chemical characterization and sources of submicron
1015 aerosols in Lhasa on the Qinghai–Tibet Plateau: Insights from high-resolution mass spectrometry,
1016 *Science of The Total Environment*, 152866, 10.1016/j.scitotenv.2021.152866, 2022.

1017 Zhao, Z., Cao, J., Shen, Z., Xu, B., Zhu, C., Chen, L.-W. A., Su, X., Liu, S., Han, Y., Wang, G., and Ho,
1018 K.: Aerosol particles at a high-altitude site on the Southeast Tibetan Plateau, China: Implications for
1019 pollution transport from South Asia, 118, 11,360-311,375, <https://doi.org/10.1002/jgrd.50599>, 2013.

1020 Zhong, M. and Jang, M.: Dynamic light absorption of biomass-burning organic carbon photochemically
1021 aged under natural sunlight, *Atmos. Chem. Phys.*, 14, 1517-1525, 10.5194/acp-14-1517-2014, 2014.

1022 Zhong, M., Xu, J., Wang, H., Gao, L., Zhu, H., Zhai, L., Zhang, X., and Zhao, W.: Characterizing water-
1023 soluble brown carbon in fine particles in four typical cities in northwestern China during wintertime:
1024 integrating optical properties with chemical processes, *Atmos. Chem. Phys.*, 23, 12609-12630,
1025 10.5194/acp-23-12609-2023, 2023.

1026 Zhu, C.-S., Qu, Y., Huang, H., Shi, J.-L., Dai, W.-T., Zhang, N.-N., Wang, N., Wang, L.-Y., Ji, S.-S., and
1027 Cao, J.-J.: Brown Carbon From Biomass Burning Reinforces the Himalayas and Tibetan Plateau
1028 Warming, *Geophysical Research Letters*, 51, e2023GL107269,

1029 <https://doi.org/10.1029/2023GL107269>, 2024.

1030 Zhu, C.-S., Cao, J.-J., Hu, T.-F., Shen, Z.-X., Tie, X.-X., Huang, H., Wang, Q.-Y., Huang, R.-J., Zhao, Z.-
1031 Z., Močnik, G., and Hansen, A. D. A.: Spectral dependence of aerosol light absorption at an urban
1032 and a remote site over the Tibetan Plateau, *Science of The Total Environment*, 590-591, 14-21,
1033 <https://doi.org/10.1016/j.scitotenv.2017.03.057>, 2017.

1034 Zhu, C. S., Qu, Y., Huang, H., Chen, J., Dai, W. T., Huang, R. J., and Cao, J. J.: Black Carbon and
1035 Secondary Brown Carbon, the Dominant Light Absorption and Direct Radiative Forcing
1036 Contributors of the Atmospheric Aerosols Over the Tibetan Plateau, *Geophysical Research Letters*,
1037 48, 10.1029/2021gl092524, 2021.

1038